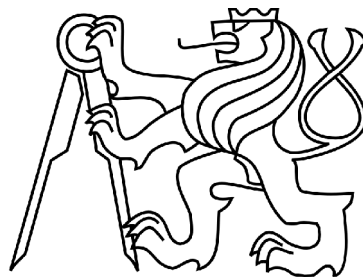


CZECH TECHNICAL UNIVERSITY IN PRAGUE
FACULTY OF CIVIL ENGINEERING
Department of Steel and Timber Structures



BACHELOR THESIS
Timber-Concrete Composite Structures

Václav Nežerka

2010

Supervisor: Doc. Ing. Petr Kuklík, CSc.

Honesty Declaration

I declare that this bachelor thesis has been carried out by me and only with the use of materials that are stated in the literature sources.

Prague, 14 May 2010

Václav Nežerka

.....

Acknowledgement

I would like to thank my supervisor, Associate Professor Petr Kuklík, who believed in me, introduced me to the issues of timber engineering and also for an opportunity to work for him as a student researcher. I also want to acknowledge the efforts of Professor Petr Kabele to provide me with a lot of valuable information regarding numerical modelling.

Special thanks go to my friend Michael Somr for his advice and willingness to discuss any problem I encountered during the writing of this thesis and my parents for their continuous support and tolerance.



ČESKÉ VYSOKÉ UČENÍ TECHNICKÉ V PRAZE

Fakulta stavební
Tháškurova 7, 166 29 Praha 6

ZADÁNÍ BAKALÁŘSKÉ PRÁCE

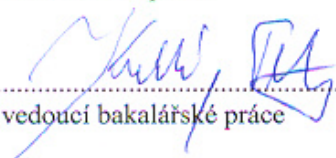
studijní program: Civil Engineering
studijní obor: Building Structures
akademický rok: 2009/2010

Jméno a příjmení studenta: Václav Nežerka
Zadávající katedra: Katedra ocelových a dřevěných konstrukcí
Vedoucí bakalářské práce: Doc.Ing. Petr Kuklík, CSc.
Název bakalářské práce: Dřevobetonové kompozitní konstrukce
Název bakalářské práce
v anglickém jazyce: Timber-Concrete Composite Structures
Rámcový obsah bakalářské práce: Esej

Datum zadání bakalářské práce: 16.2.2010 Termín odevzdání: 14.5.2010
(vyplňte poslední den výuky příslušného semestru)

Pokud student neodevzdal bakalářskou práci v určeném termínu, tuto skutečnost předem písemně zdůvodnil a omluva byla děkanem uznána, stanoví děkan studentovi náhradní termín odevzdání bakalářské práce. Pokud se však student řádně neomluvil nebo omluva nebyla děkanem uznána, může si student zapsat bakalářskou práci podruhé. Studentovi, který při opakovaném zápisu bakalářskou práci neodevzdal v určeném termínu a tuto skutečnost řádně neomluvil nebo omluva nebyla děkanem uznána, se ukončuje studium podle § 56 zákona o VŠ č. 111/1998. (SZŘ ČVUT čl. 21, odst. 4)

Student bere na vědomí, že je povinen vypracovat bakalářskou práci samostatně, bez cizí pomoci, s výjimkou poskytnutých konzultací. Seznam použité literatury, jiných pramenů a jmen konzultantů je třeba uvést v bakalářské práci.


vedoucí bakalářské práce


vedoucí katedry

Zadání bakalářské práce převzal dne: 17.2.2010


student

Formulář nutno vyhotovit ve 3 výtiscích – 1x katedra, 1x student, 1x studijní odd. (zašle katedra)

Nejpozději do konce 2. týdne výuky v semestru odešle katedra 1 kopii zadání BP na studijní oddělení a provede zápis údajů týkajících se BP do databáze KOS.

BP zadává katedra nejpozději 1. týden semestru, v němž má student BP zapsanou.
(Směrnice děkana pro realizaci studijních programů a SZZ na FSv ČVUT čl. 5, odst. 7)

Abstract

This thesis provides an analytical calculation of a load-bearing capacity for a timber-concrete composite T-beam with shear connectors at room temperature and at elevated temperatures during fire. For such calculation it is possible to develop an application, for instance in a well available MS Excel.

Fire design of timber-concrete composites is not described in standards, even though the fire safety has become a much-discussed issue, in particular with an increasing popularity of timber and timber-concrete composite structures.

To simulate the behaviour of timber-concrete composite structure is a very complex task. It requires knowledge of structural behaviour of composite structures with interlayer slip and behaviour of timber beams, concrete layer and steel connectors exposed to high temperatures.

Data from experiments, amended by results from numerical models, provided a valuable data for verification of results given by analytical calculation.

Keywords: timber-concrete composite, partial composite action, shear connectors, heat transfer, fire resistance

Abstrakt

Tato práce poskytuje analytický výpočet statické únosnosti spřaženého dřevobetonového nosníku za pokojové teploty a také za zvýšených teplot při požáru. Pro takový výpočet je možné naprogramovat aplikaci, například pomocí běžně dostupného programu MS Excel.

Požární návrh kompozitních spřažených konstrukcí není popsán v normách, přestože požární bezpečnost se stala velmi diskutovaným problémem, zejména ve spojení s rostoucí popularitou dřevěných a dřevobetonových konstrukcí.

Simulace chování dřevobetonové konstrukce je velmi složitá, jelikož vyžaduje znalost statického působení kompozitních konstrukcí s prokluzem a chování dřevěných trámů, betonové desky a spřahovacích prostředků za zvýšené teploty.

Výsledky experimentů, doplněné výpočty numerických modelů, poskytly cenná data pro ověření výsledků analytického výpočtu.

Klíčová slova: dřevobeton, částečné spřažení, spřahovací prostředky, prostup tepla, požární odolnost

Contents

1 Introduction	7
1.1 History	8
1.2 Recommendations for Construction	8
2 Timber-Concrete Composites Nowadays	10
2.1 Refurbishment of Old Timber Floors	11
3 Goals	12
4 Mathematical Formulation of Partial Composite Action	13
4.1 Differential Equation for Partial Composite Action for Elastic Analytical Model	14
5 Shear Connectors For Timber-Concrete Composites	17
5.1 Dowel-Type Connectors	18
5.2 Metal Plate Connectors	19
5.3 Shear Key/Anchor Connection	20
5.4 Continuous Glued-in Plate	21
6 Design of Timber-Concrete Composite Floors	23
6.1 Ultimate Limit State	23
6.2 Simplified Design Method (γ -Method)	24
6.2.1 Basic Assumptions and Determinations	24
6.2.2 Determination of Moment Resistance	27
6.2.3 Determination of Shear Resistance:	29
6.2.4 Determination of Fastener Bearing Capacity	31
6.3 Comparison of Results with Laboratory Tests and Numerical Models	32
6.4 Serviceability Limit State	34
6.4.1 Instantaneous Bending Stiffness ($t = 0$).....	34
6.4.2 Long-Term Bending Stiffness ($t = \infty$)	34
7 Fire Design of Timber-Concrete Composite Floors	36
7.1 Mechanical Loading During Fire.....	36
7.2 Nominal Temperature-Time Curves.....	37
7.3 Behaviour of Timber in Fire	38
7.3.1 Basic Assumptions and Determinations for Calculation.....	39
7.4 Behaviour of Shear Connectors at Elevated Temperature.....	40
7.5 Behaviour of Concrete at Elevated Temperature.....	42
7.5.1 Determination of Temperature within Concrete Layer	42
7.5.2 Cross-Section Temperature According to Analytical and Numerical Model.....	45
7.5.3 Load-Bearing Capacity of Concrete Component at Elevated Temperature	49
7.6 Strength and Stiffness of the Composite Cross-Section	50
7.7 Comparison of Results with Full-Scale Laboratory Tests.....	51
8 Comparison of Timber-Concrete Composite and RC Floor	53
8.1 RC Floor Design and Performance.....	53
8.2 Design and Performance of Timber-Concrete Composite Floor.....	54
8.2.1 Cross-Section Optimization for Better Performance in Fire	57
9 Conclusion	59
Notation	60
References	62

1 Introduction

Traditionally, timber has been used mainly for residential buildings. However, in past years structural engineers have been researching and developing a timber and concrete composite scheme that enables large open-plan buildings to be constructed with a timber. The system locks concrete floor to timber beams using shear studs or by other means of shear connection.

In comparison with timber-concrete composite, reinforced concrete is highly wasteful solution. The tensile zone cracks allowing moisture to enter leading to corrosion, spalling and other types of deterioration, and about 40-60% of the depth is ineffective, only holding rebar in place. Moreover, the steel rebar is more expensive than timber. In addition, the exposed rebar is a potential fire protection problem. Moreover, timber-concrete composite floors are much more efficient than all-reinforced concrete systems in terms of load carried per unit self-weight. These floor systems are competitive compared to all-concrete floors, based on total cost, owing to factors such as rapid construction, less concrete formwork and less shoring needed during construction (because timber elements can partly provide this), and finally reduced foundations because of the low self-weight.

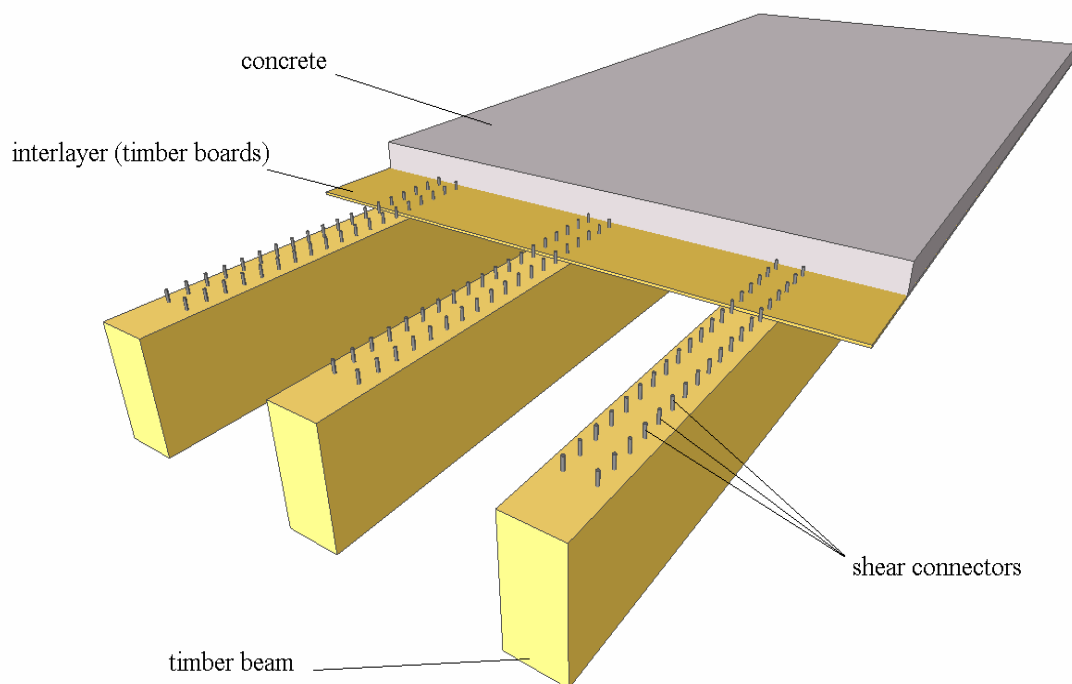


Figure 1.1: Typical composition of the beam-type floor using glulam or solid timber beams

The environmental arguments are also persuasive. Timber requires less energy and produces less carbon dioxide in its manufacture. Without taking into account the carbon that trees remove from atmosphere during growth, there has been carried out a research comparing the embodied carbon dioxide in steel, concrete and timber frames. For a 900 square metres building, excluding the foundations, which would be comparable for all three, concrete and

steel come out more or less identical at about 1 800 tonnes of embodied carbon dioxide, while timber frame has 875 tonnes.

The concrete slab also brings the benefit of thermal mass, which can be exploited to help to regulate the internal temperature in the building. A negative implication of the composite scheme is that the building becomes more difficult to deconstruct.

The research has shown that a composite timber and concrete beam is twice strong and three times stiffer than a timber beam acting independently. This results in less timber being used in the building. The timber can also be designed to char, providing some portion of fire resistance, which can be extended by using of bigger timber beams. Durability can be achieved by using treatments or by specifying more durable timbers such as larch. While the second solution may be more expensive, a life-cycle costing may prove this to be the more economic solution.

1.1 History

The first development of a timber-concrete composite system was caused by a shortage of steel for the reinforcement of concrete after both world wars. Gerber et al (1993) mention a patent of Müller (1922), in which a system of nails and steel braces form the connection between a concrete slab and timber.

Poštulka (1983, 1997) mentions more than 10 000 m² of timber floors that have been refurbished with the timber-concrete system in the CSSR since 1960. Nails 180 mm long with diameter 6,3 mm that are spaced 100 mm near supports and 250 mm at mid-span, form the connection between concrete and timber.

Timber concrete composite bridges that were built in New Zealand since 1970 are described by Nauta (1984). A 150 mm thick reinforced concrete slab is used where traffic is reasonably heavy. By using this type of slab in composite structure with glulam beams, the size of the beams can be reduced by 20 percent.

The first publication that combined the theory and practice of refurbishment of existing timber floors by adding a concrete slab was by Godycki et al (1984). Thousand square metres of existing timber floors were refurbished by this method in Lods, Poland, in 1981. Most timber beams could be reused within the composite system. The cost of the timber-concrete composite system was only half the cost of the alternative refurbishment methods.

1.2 Recommendations for Construction

- a) Do not use wet timber. If this is unavoidable, use timber without pith, or make sure that cracks do not affect the location of fasteners.
- b) Leave propping (shoring) in place for longer than required for all-concrete systems. It is important to meet this requirement in order to avoid excessive initial deflection of the composite floor.
- c) Use corrosion-protected fasteners (zinc-coated steel or stainless steel).
- d) Reinforce the concrete, especially if thick concrete sections are being designed, in order to avoid loss of stiffness due to large cracks on the tension part of the concrete slab.
- e) Protect the timber from moisture when casting the concrete, i.e. by using plastic layers or concrete with additives that reduce the water/cement ratio. A lower water/cement ratio has also the benefit of reducing concrete shrinkage.
- f) Avoid timber species with adverse chemical reaction to cement, e.g. larch which is a species with high-sugar-content extracts.

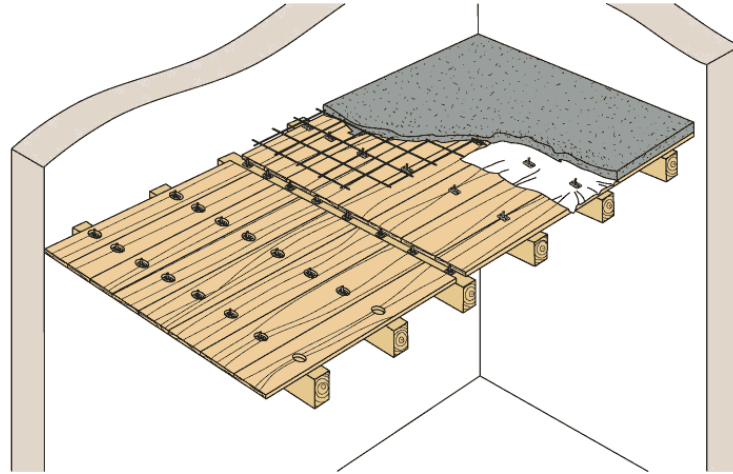


Figure 1.2: Typical composition of timber-concrete composite floor

In case of refurbishment of old timber floors it is possible to use original timber beams. It is usually required to change old timber decking and treat the beams with fungicides and insecticides. Then the shear connectors are fixed to the timber beams, reinforcing mesh is put above the timber decking (see figure 1.3) and concrete with a low water/cement ratio is poured in a required thickness. Temporary shoring must provide a support the timber beams until the concrete hardens.



Figure 1.3: Before pouring of concrete it is necessary to put reinforcing mesh preventing development of cracks at the lower surface of a concrete slab

2 Timber-Concrete Composites Nowadays

Use of timber-concrete composite floors can be found in construction of new multi-storey houses with timber frame or cross-laminated panels as a vertical load-bearing structure. The key component of a multi-storey timber building is the floor system. There are several specific requirements such as: resistance to gravity load (strength limit state for out-of-plane loading), control of vibration and deflection due to gravity load (serviceability limit state), (3) resistance to lateral load (strength limit state for in-plane loading), (4) control of deflection due to lateral load on the diaphragm (strength and serviceability limit state), (5) fire resistance, (6) acoustic separation, and (7) thermal insulation.

Timber-concrete composite floors have such large in-plane rigidity that they keep their shape (and consequently the shape of the entire building) during an earthquake. This permits use of simplified seismic analysis procedures. Of course, it is necessary that both, the timber ribs and the concrete slab layer, have a good connection to masonry walls.

Traditional joist floors are extensively used for single- or two-storey houses. Such flooring is constructed from particleboard or plywood nailed to timber joists and blocking. The system is light, easy to construct and inexpensive, however, it does not fulfil all of the aforementioned performance requirements especially in terms of deflection and vibration for medium to long spans, and acoustic separation. Such disadvantages have over the years resulted in the investigation and introduction of different innovative systems in several parts of the world, such as the stressed skin panels in Australia, cross-laminated timber in Austria, and timber-concrete composite floors in Europe, United States Australia.



Figure 2.1: Timber and concrete composite schemes also enable large open-plan buildings to be constructed primary beams are then made of steel or glulam timber with a large cross-section

2.1 Refurbishment of Old Timber Floors

There is also increasing significance of the protection and reconstruction of old and historic buildings in modern planning. Therefore, an efficient type of floor system which consists of timber members in the tensile zone, a thin concrete layer in compression zone and the connection between timber and concrete has drawn attention of the experts in the field of civil engineering. The advantage of such refurbishment is that an existing timber floor can remain intact and is strengthened by adding of a concrete slab. The results of such reconstruction-strengthening procedure are (1) retaining the original timber structures and simultaneously increasing its stiffness and strength, (2) developing a rigid floor diaphragm, and (3) enhancing the acoustic separation, thermal mass, and fire resistance of the floor.

First condition for the usage of a timber-concrete composite floor is a reasonably good health of timber beams. It is strongly recommended to carry out a comprehensive survey of the floor structure, including a mycological one. It is necessary to investigate the measure of timber infestation by insects and fungal attack. Damaged parts of the beam have to be replaced and the entire floor structure has to be protected by fungicide paint or other by means of other fungicidal agents.



Figure 2.2: Comprehensive survey should be carried out before the strengthening of the old floor structure

3 Goals

The goal of this bachelor thesis is to analyze behaviour of timber-concrete composite beams at room and elevated temperatures. It is particularly focused on:

- description of different connector-types ensuring the composite action
- structural behaviour of timber-concrete composites
- analytical model of ULS and SLS design at room temperatures
- establishment of an analytical model at elevated temperatures during fire
- programming of an Excel application a for calculation of a timber-concrete composite beam at room and elevated temperatures
- verification of results given by the analytical models using the FEM and data from experiments
- comparison of the performance of timber-concrete composite and reinforced concrete floor at fire situation
- optimization of a cross-section for a better performance in fire

4 Mathematical Formulation of Partial Composite Action

If subjected to bending, adjacent layers of semi-rigid systems slide relative to one another in a partially constrained manner, with relative slip being maximum at the points with maximum shear force and without slip at the points with zero shear force (in case of simply supported beam loaded by uniform symmetric loading, the location of such point is in the middle of the beam). Such behaviour is described in the figure 4.1.

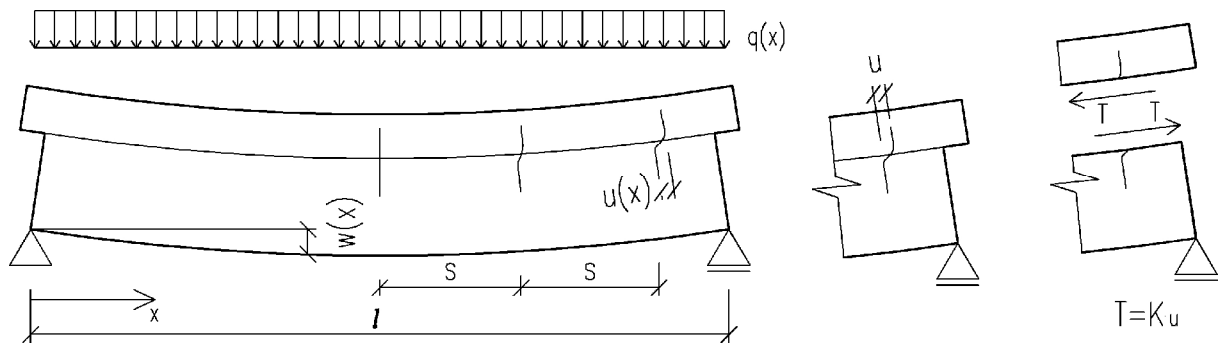


Figure 4.1: Behaviour of a composite beam with semi-rigid connection

Classical bending theory of beams cannot be applied in unmodified form because of this slip. The mechanism is easily explained in terms of a two-layer, simply supported composite beam with uniform construction throughout its length. When loaded, such beam develops a system of forces on fasteners T , that are tangential to the interface between layers, with T at any location being related to the amount of slip in the fastener(s) at that location, see figure 4.1.

T forces ensure equilibrium of each layer in the axial direction in a manner that is locally and globally consistent with deformation. Because slip u is maximal at the ends, T is also maximal there. For a fully symmetric arrangement both quantities are zero in the middle. This causes a system of balancing axial forces in the layers N_c , N_t . When a horizontal beam is loaded in pure bending so that the beam deflects downwards, N_c is compressive and N_t is tensile force. Both, N_c and N_t are diminishing at the ends and maximal in the middle of the beam. These forces act as an internal couple of forces, their intensity depends on the stiffness of fasteners (it would be zero if there were no connection between layers). The total bending moment at a cross-section equals to the sum of local bending moments in the layers $M_c + M_t$ and the moment developed by force couple involving N_c and N_t .

$$N_c = N_t = N \quad M = M_c + M_t + N \cdot r \quad (4.1)$$

If the rigidity of the connection is increased, local bending moments in the layers decrease, and axial forces N_c and N_t must increase. The decrease in $M_c + M_t$ reflects the fact that increased connection stiffness reduces the beam deflection, which in return reduces the radius of curvature.

The load on an individual fastener in a connection T at slip u is:

$$T = K \cdot u \tag{4.2}$$

where K is the “slip modulus”, determined by testing. Because connections between layers are assumed to be continuous, the “slip modulus per-unit-length” $k = K / s$, rather than K is used in analysis (s is spacing between connectors). There exist closed-form solutions for predicting distributions of T , N , flexural rigidity and stresses in layers if the response of the system is linear-elastic, shear deformation in the layers is negligible and k is uniform along the beam.

4.1 Differential Equation for Partial Composite Action for Elastic Analytical Model

The model discussed in this paragraph is closely related to Möhler’s model (1956). The basic assumptions of this model are:

- a) a linear elastic material behaviour is assumed for concrete and timber, cracking and plasticity are thus not taken into account,
- b) the connectors are equally spaced,
- c) all connectors have the same load-slip relationship that is linear elastic up to the load-bearing capacity of the connector and from that point on ideal plastic behaviour is assumed (in this model only the elastic part is used and a maximum strength is not given, each connector type is only described by its slip modulus K),
- d) the discrete connectors are assumed to act as a continuous connection, called “smeared” connectors, with slip modulus k ,
- e) the friction between the timber and the concrete is not considered, the shear force in the interlayer is totally taken by its connectors.

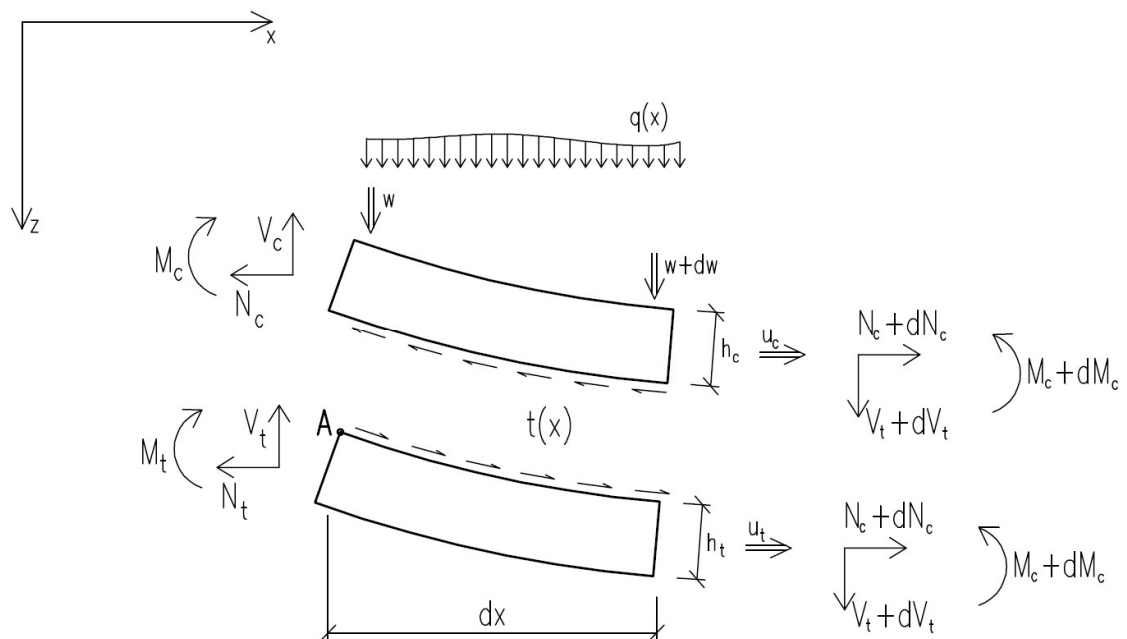


Figure 4.2: Part of the composite beam loaded by $q(x)$

Equilibrium between internal and external forces on figure 4.2 yields:

$$\downarrow F_z(x) = 0 \Rightarrow \frac{dQ_c(x)}{dx} + \frac{dQ_t(x)}{dx} = -q(x) \quad (4.3)$$

$$\rightarrow F_x(x) = 0 \Rightarrow \frac{dN_c(x)}{dx} + \frac{dN_t(x)}{dx} = 0 \quad (4.4)$$

$$\sum M_A(x) = 0 \Rightarrow \frac{dM_c(x)}{dx} + \frac{dM_t(x)}{dx} - \frac{dN_c(x)}{dx} \cdot \frac{h_c}{2} - \frac{dN_t(x)}{dx} \cdot \frac{h_t}{2} = Q_c(x) + Q_t(x) \quad (4.5)$$

the last equation can be written as

$$\sum M_A(x) = 0 \Rightarrow \frac{dM_c(x)}{dx} + \frac{dM_t(x)}{dx} - \frac{dN_c(x)}{dx} \cdot \frac{h}{2} = Q_c(x) + Q_t(x) \quad (4.6)$$

since

$$\frac{h_c}{2} + \frac{h_t}{2} = \frac{h}{2} \quad \text{and} \quad \frac{dN_c(x)}{dx} = \frac{dN_t(x)}{dx} \quad (4.7)$$

Above mentioned equilibrium equations were combined with the constitutive equations for normal force and bending of the two elements, resulting in:

$$(EI_c + EI_t) \frac{d^4 w(x)}{dx^4} + EA_c \cdot \frac{d^3 u_c(x)}{dx^3} \cdot \frac{h}{2} = q(x) \quad (4.8)$$

The contribution of the normal forces in each component is given by:

$$-EA_c \cdot \frac{d^2 u_c(x)}{dx^2} = k \quad u(x) = k \cdot [u_t(x) - u_c(x)] + k \cdot \frac{dw(x)}{dx} \cdot \frac{h}{2} \quad (4.9)$$

$$-EA_t \cdot \frac{d^2 u_t(x)}{dx^2} = k \quad u(x) = k \cdot [u_t(x) - u_c(x)] + k \cdot \frac{dw(x)}{dx} \cdot \frac{h}{2} \quad (4.10)$$

which results in three equations with three parameters to be solved:

- 1) $w(x)$, the deflection in z-direction,
- 2) $u_c(x)$, the displacement at the centre of gravity of the concrete in x-direction, and
- 3) $u_t(x)$, the displacement at the centre of gravity of the timber in x-direction.

A simple closed form solution is obtained for a load:

$$q(x) = q_0 \cdot \sin\left(\frac{\pi}{l} \cdot x\right) \quad (4.11)$$

By stating

$$w(x) = C_1 \cdot \sin\left(\frac{\pi}{l} \cdot x\right) \quad (4.12)$$

the constant C_1 is calculated as

$$C_1 = \frac{q_0 \cdot l^4}{\pi^4 \cdot EI_{eff}} \quad (4.13)$$

with

$$EI_{eff} = E_t \cdot \left[I_{tot} + \gamma \cdot (n_c \cdot A_c \cdot z_c^2 + A_t \cdot z_t^2) \right] \quad (4.14)$$

$$\text{where } n_c = \frac{E_c}{E_t} \quad \text{and} \quad I_{tot} = I_t + n_c \cdot I_c$$

where z_c is the distance from overall neutral axis to the centre of gravity of the concrete layer; z_t is distance from overall neutral axis to the centre of timber beam; the connection efficiency factor (γ_{ct}) can be expressed as:

$$\gamma = \frac{1}{1+p} \quad \text{where} \quad p = E_c \cdot \left(\frac{\pi}{l}\right)^2 \cdot \frac{1}{k} \cdot \frac{A_t \cdot A_c}{A_t + n_c \cdot A_c} \quad (4.15)$$

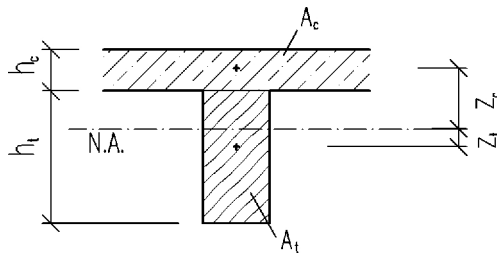


Figure 4.3: Eccentricities and cross-sectional areas of the concrete slab and timber beam

5 Shear Connectors For Timber-Concrete Composites

The behaviour of timber-concrete composite slabs is essentially influenced by the shear connection between timber and concrete. Therefore the shear connector is a critical component of the system and, to a great extent, determines the performance of the system.

The function of the shear connector is to effectively transfer the shear between the wood beam and the concrete deck to promote composite action. There are two bounds of composite action: a lower bound where the layers are not connected and work independently (no composite action) and an upper bound where the two layers are rigidly connected with no interlayer slip (full composite action). Of course, the second case is the desirable one, however, no slip is difficult to achieve and most connectors produce at least some interlayer slip (partial composite action). Minor slippage can be beneficial, allowing distribution of shear stresses along the shear connectors. The low connection stiffness is required in cases, where big hygrothermal volume changes may occur, because response on the temperature and especially moisture significantly differs for the timber and concrete components.

In order to design composite section, it is critical to know the shear connector capacity and failure mode. Due to relatively non-ductile failure modes of the constituent concrete (compression) and timber (tension), ductile failures in the shear connector may provide increased overall ductility and reliability. The resulting composite system produces increased strength, stiffness, ductility, reliability, and long-term performance as compared to similar non-composite section.

A big amount of shear connection systems exist. They are perhaps best categorized into four groups: dowel-type, metal plate, shear key/anchor connections, and finally glued-in plate connectors.



Figure 5.1: Shear test setup

5.1 Dowel-Type Connectors

Connections included in this group have the advantage of being inexpensive and uncomplicated to install. However, they are generally considered to be the least rigid of all systems and usually provide, in comparison with other systems, quite low ductility of the shear connection.

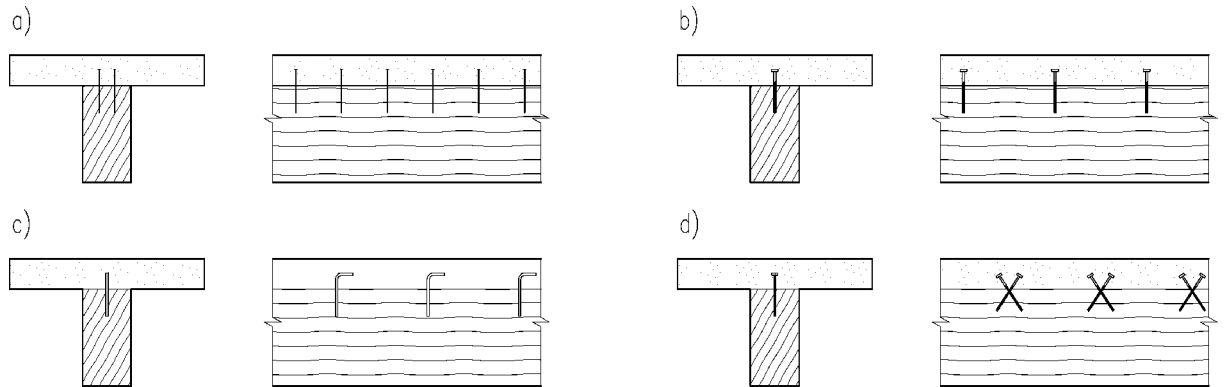


Figure 5.2: Dowel-type connectors: a) nails, b) screws (vertical arrangement), c) glued rebar, d) screws (inclined)

By arranging the screws at $\pm 45^\circ$ inclination (see figure 5.2 d) a virtual truss is formed with timber and concrete as chords and connectors as diagonals (figure 5.3). The model in figure 3 was done in ADINA Structures software. The connectors are replaced by a continuum made of steel with equal stiffness. As indicated by vectors of principal stresses, the idea of formation of a virtual truss with one screw in tension and second in compression seems to be very good solution.

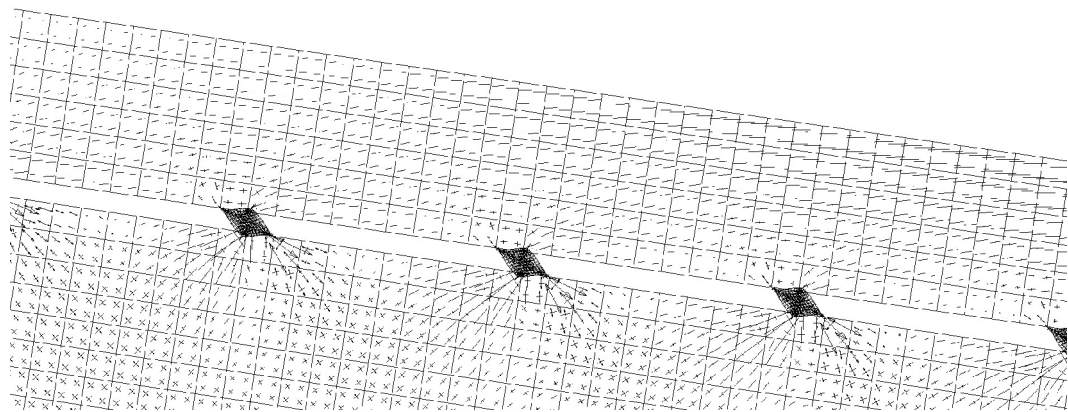


Figure 5.3: Direction of principal stresses in connection

According to Timmermann and Meierhofer (1993), such arrangement improves the stiffness by a factor about 3 compared to a vertical arrangement where the connectors act in bending. There a quite satisfactory rigidity can be reached in a simple way, utilizing maximally the available connectors.

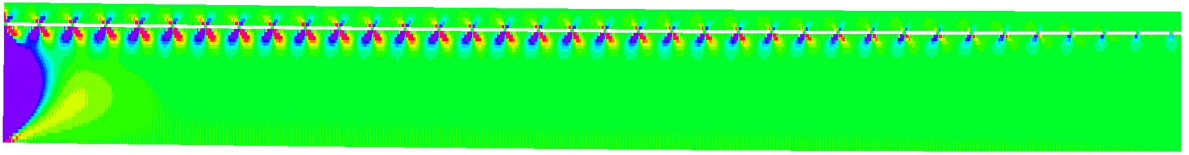


Figure 5.4: Shear transfer in composite beam

As indicated in figure 5.4, the shear connectors are most loaded near supports while those in the midspan (the right part of the picture) are unloaded. The force transferred by fasteners varies according to shear force diagram.



Figure 5.5: Slip in the screw connector with a vertical arrangement

The failure of dowel-type connector with a vertical arrangement is considered in Eurocode to be exclusively due to the loss of bearing capacity of a timber element and therefore the formula for calculation of a load-bearing capacity per one fastener is derived from the formula for connection of two timber elements multiplied by factor 2,0.

This means that only failure of bearing in timber is taken into account and the connector is rigidly fixed in a concrete layer. However, according to the laboratory tests conducted at the Czech Technical University in Prague, this is not 100% true, since a small deformation (local cracking) in concrete also appears. Therefore the factor should be less than 2,0 for the safe calculation.

5.2 Metal Plate Connectors

These connectors have higher stiffness, ductility and ultimate strength than dowel-type connectors (Blaß and Schlager 1996). The reason is that nails and screws typically cause wood splitting failure, whereas plate connectors can cause failure in wood embedment, steel shear, or concrete crushing.

Regarding a fire resistance, the punched metal plate fasteners are exposed to fire and therefore this system is not suitable.

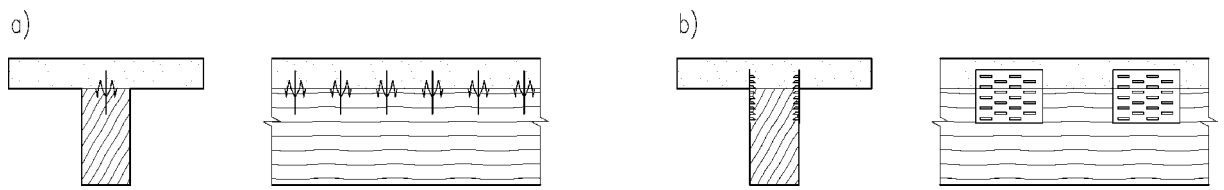


Figure 5.6: Metal plate connectors: a)toothed plate, b)steel punched metal plates



Figure 5.7: Yielding of plate takes place after cracks in concrete appear

5.3 Shear Key/Anchor Connection

The intent of the shear key/anchor detail is to achieve interlayer shear transfer by bearing stresses in timber and horizontal shear in the concrete key. Notches are cut into the wood and reinforced with an anchoring device such as a post-tensioned bolt or lag screw. These connectors have been shown to have similar to moderately better strength and slip resistance than group of metal plate connectors (Blaß and Schlager 1996).

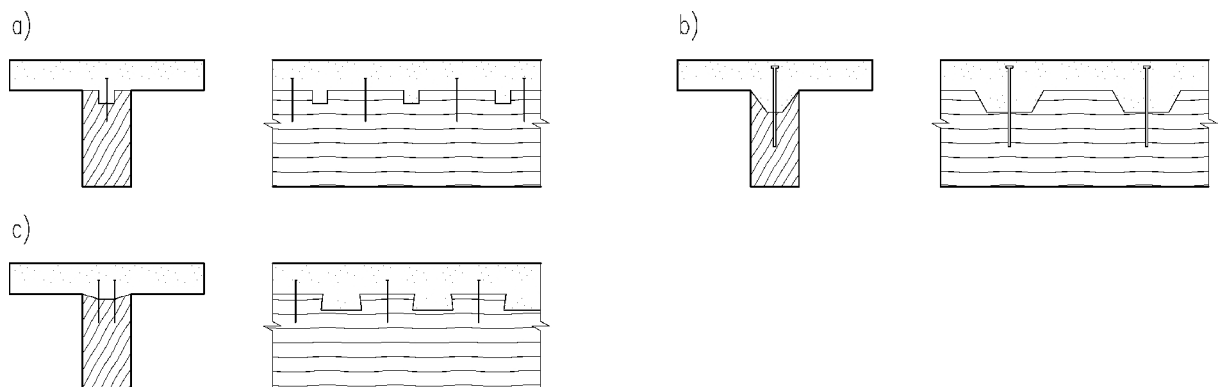


Figure 5.8: Shear key/anchor connections: a)round notches in timber with fasteners preventing uplift, b)cup notches and prestressed steel bars, c)square notches with fasteners preventing uplift

The horizontal shear forces are transferred through the shear key with little interlayer slip, while the dowels work in tension to resist the vertical load component. Thus, the anchor connector itself is not subjected to shear

Gutkowski et al. (2000) reported the load-slip response to be initially linear with abrupt partial failure (presumably of the concrete) with a modest residual ductile behaviour thereafter (presumably from yielding of the dowel).

To avoid a right angle notch that might split at the base, it is good to make the angular cut of the shear key at 75 degrees from the vertical.

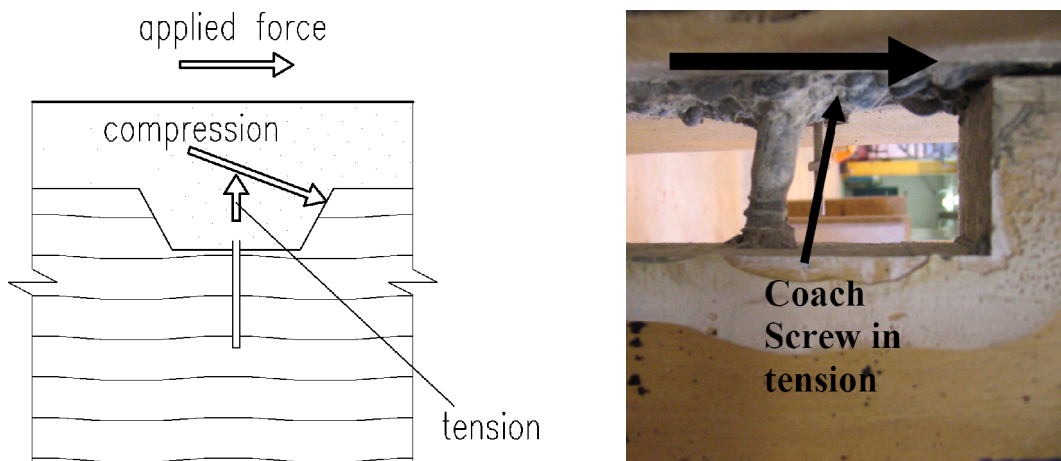


Figure 5.9: Scheme of the forces in the connection and photo of a deformed connector

5.4 Continuous Glued-in Plate

Connectors in this group are generally considered to possess the greatest rigidity (Ceccotti 1995). The observed failure modes from experimental shear tests are reported as primarily wood shear failure or steel plate failure (Bathon and Graf 2000). For design purposes, interlayer slip is often considered negligible and in the case of bending, the assumption of plane sections remaining plane is generally accepted.

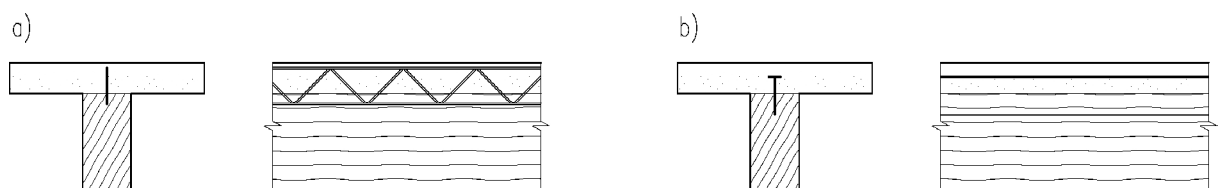


Figure 5.10: Continuous glued-in plate connectors: a) steel lattice glued to timber, b) steel plate glued to timber

Consequently, design calculations for this group of connectors may be easily done through transformed sections. In this regard, glued-in plate connectors present a design advantage over other connector types.

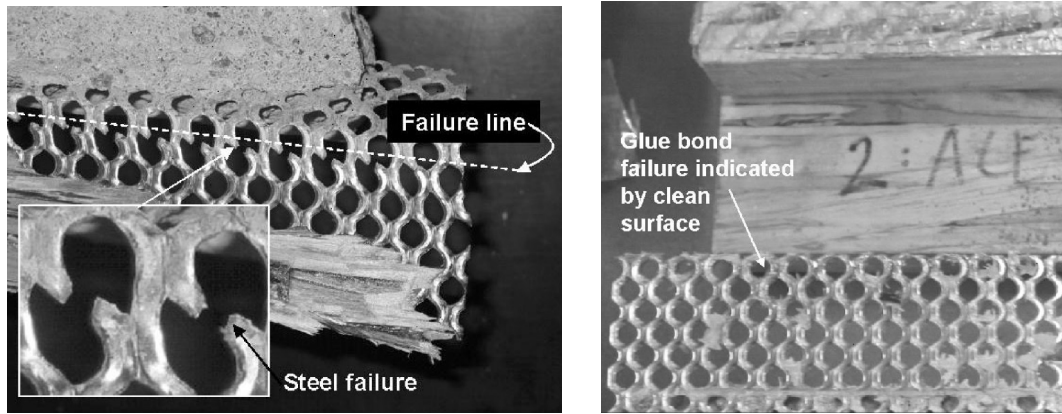


Figure 5.11: Failure of the continuous mesh indicated by failure mode (left) and failure of the glue bond (right)

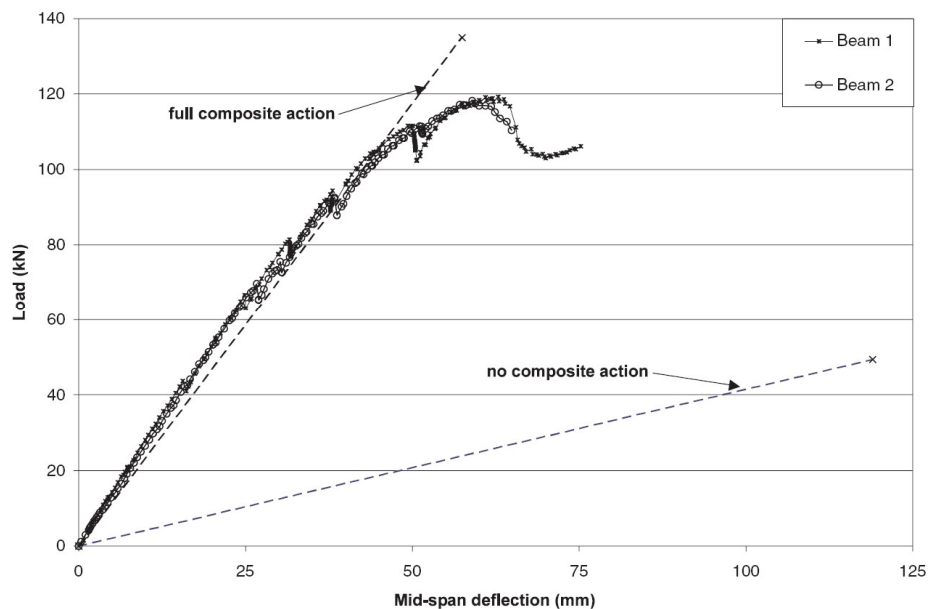


Figure 5.12: Full-scale test proved no-slip behaviour of the connection (Clouston, Civjan, Bathon, University of Massachusetts)

There are many producers of different systems providing the data about their products obtained from testing of sufficient amount of specimens. Groups mentioned above give only the overview of basic principles for the shear connection in timber-concrete composites.

6 Design of Timber-Concrete Composite Floors

For timber-concrete composite members subjected to a positive bending moment the timber members are subjected to combined bending and tension, the concrete layer to combined bending and compression (see figure 6.1). The function of the connectors is to transfer the shear force between the subcomponents (timber and concrete). The shear force, which is in equilibrium with internal normal forces of the subcomponents, depends on the stiffness of the shear connection. Without connection the timber and concrete subcomponents should be considered as independent members subjected only to bending ($N = 0$).

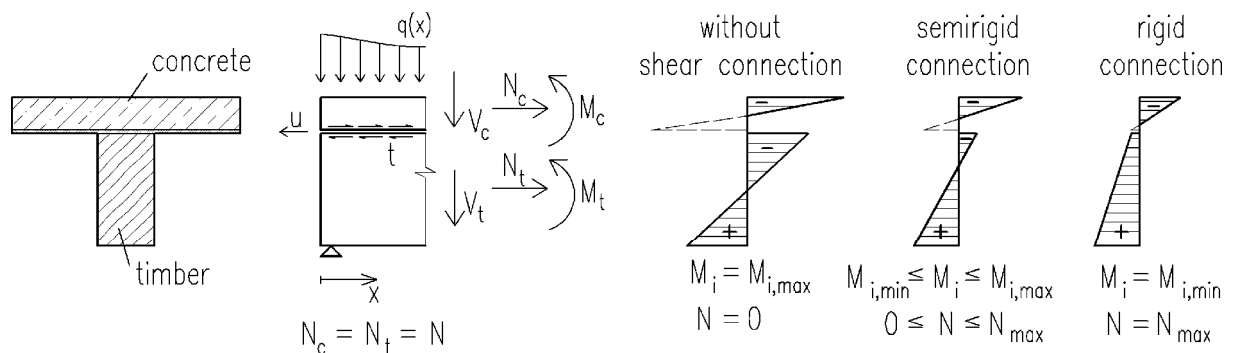


Figure 6.1: Stress distribution of a timber-concrete composite beam depending on the rigidity of the timber-concrete connection

A rigid connection develops full composite action between the subcomponents. Since no slip between the timber and concrete occurs, the composite structure should be considered as one unit and therefore conventional principles of the structural analysis can be applied. For a rigid connection the subcomponents are subjected to the maximal internal force $N = N_{\max}$, and to the minimal internal bending moments ($M_i = M_{i,\min}$).

A semi rigid connection, on the other hand, develops only partial composite action and therefore the structural analysis requires a consideration of an interlayer slip between the subcomponents. For a partial composite action the Bernoulli's hypothesis is not applicable for the cross-section as a whole. However, the assumption that plane sections remain plane after the deformation is still valid for each subcomponent. The full composite action (infinite slip stiffness) and no composite action (zero slip stiffness) represent therefore the upper and lower bound for the partial composite action.

The structural behaviour of timber-concrete composite members is governed by the shear connection between timber and concrete. If the connection strain remains in the linear elastic range until the timber members fail, linear-elastic behaviour of the composite structure may be assumed. If, on the other hand, the connectors reach their load carrying-capacity, the outer connectors will deform plastically and a non-linear behaviour of the composite structure should be considered.

6.1 Ultimate Limit State

In design codes and standards for timber, elastic analysis is allowed for predicting ultimate limit states. This means that not only timber is assumed to respond linear elastically, but also

concrete and connectors will deform only in elastic range, even though both, concrete and connections can exhibit nonlinear behaviour. Since predictions are on the safe side, secant moduli are adopted for concrete and connections as an indirect means of accounting for inelastic deformation.

In global analysis normal force and moment in the concrete slab and timber ribs, the concrete is considered uncracked. This means that the second moment of area I_{eff} for the entire (transformed) cross-section must be considered. On the other hand, for the cross-section verification the concrete is considered to have no tensile strength. The limiting strength in compression is crushing strength of concrete. Reinforcing bars should be provided on the tension side of the slab to prevent cracking.

Connection slip modulus $K_u = 0,6F_{max} / u_{0,6}$ according to ISO 6891. Usually $K_u \approx 0,67K_{ser}$. Unless for some reason connection strength and stiffness are underestimated, these procedures work reasonably well. If connection stiffness is underestimated, linear elastic behaviour will be certainly achieved. To account fully for nonlinear behaviour of materials and connections FEA models must be used.

Constraining forces arise within composite systems when the two parts are subjected to volume changes. When concrete shrinks, the reduction in length of the concrete slab favours fasteners because it tends to reduce their deformation. On the other hand, this increases the deflection of the beam. Although this can be counteracted by giving a system precamber, most of the shrinkage happens during initial curing when the entire structure is still propped. Another phenomenon that introduces internal stresses, is the volume change of timber due to change of humidity in the surrounding environment.

When connections are very stiff and/or the span is long (e.g. in case of bridges), simple calculations suggest that hygrothermal stresses can be quite severe, and there is need for precise study of this issue. It is advisable with long spans to use relatively soft connections that minimize constraint effects in case of long spans.

6.2 Simplified Design Method (γ -Method)

For a design purposes a simplified design method for mechanically jointed beams according to Annex B of Eurocode 5, based on the differential equation for the partial composite action, is widely used.

The simplified design method, called “ γ -method” is closely related to Mohler’s model with constant slip stiffness. It was developed for simply supported beams subjected to loads giving a bending moment varying sinusoidally, because for such case the differential equation of the partial composite action has a simple analytical solution.

However, the γ -method may be used also for loads giving a bending moment varying parabolic and for a slip stiffness varying according to the shear force, because the differences between the simplified design method and an exact solution of the differential equations are not so relevant in comparison with the large variation of the mechanical properties of individual components (especially, for the E-modulus of timber and the slip-modulus of the connection).

6.2.1 Basic Assumptions and Determinations

Derivation of so called γ -method is based upon the following fundamental assumptions:

- a) Bernoulli’s hypothesis is valid for each subcomponent (shear deformation of each subcomponent can be neglected since ratio of length to height of those subcomponents is relatively high),

- b) material behaviour of all sub-components is linear elastic (which must be satisfied, since timber subjected to combined bending and tension exhibits brittle behaviour, while concrete slab is primarily subjected to compression and the timber members usually fail before a plastification of the concrete slab occurs),
- c) the distances between the dowels are constant along the beam (however, Eurocode allows varying spacing of connection according to shear force)
- d) slip modulus is taken in plastic area for ultimate limit state and elastic area for serviceability limit state (see figure 6.2),
- e) bending moment is varying sinusoidally or parabolically.

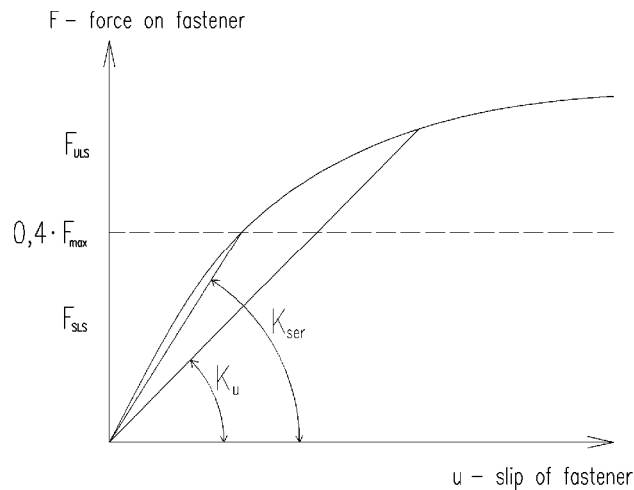


Figure 6.2: *F-u diagram of the slip in the connection*

Equation (1) shows the position of the neutral axis of the composed section with mechanically jointed elements:

$$z_t = \frac{\sum S_{y,i}^{\gamma_{ct}}}{\sum A_i} = \frac{n_c \cdot \gamma_{ct} \cdot A_c \cdot (h_t + h_c + 2 \cdot t_w)}{2 \cdot (n_c \cdot \gamma_{ct} \cdot A_c + A_t)} \quad (6.1)$$

where z_t is a position of overall neutral axis from the centre of gravity of the timber member; n_c is given by equation (6.4); γ_{ct} is a connection stiffness coefficient given by equation (6.6); A_i is the area of subcomponents; h_i is the thickness of subcomponents and t_w is the thickness of interlayer as shown in figure 6.3.

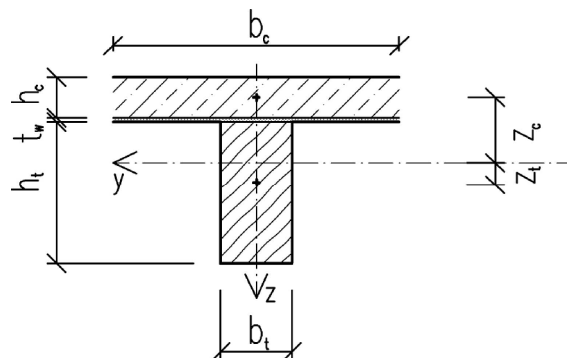


Figure 6.3: *Composite cross-section*

For calculation of the area of concrete, so called effective width b_{eff} should be used. According to Eurocode 2, the effective flange width b_{eff} for a T-beam or L-beam may be calculated as:

$$b_c = b_{eff} = \sum b_{eff,i} + b_t \leq b \quad (6.2)$$

where

$$b_{eff,i} = 0,2b_i + 0,1l_0 \leq 0,2l_0 \quad \text{and} \quad b_{eff,i} \leq b_i \quad (6.3)$$

where l_0 is a clear span between supports (i.e. between points of zero moment). For the notations of other variables see figure 6.4.

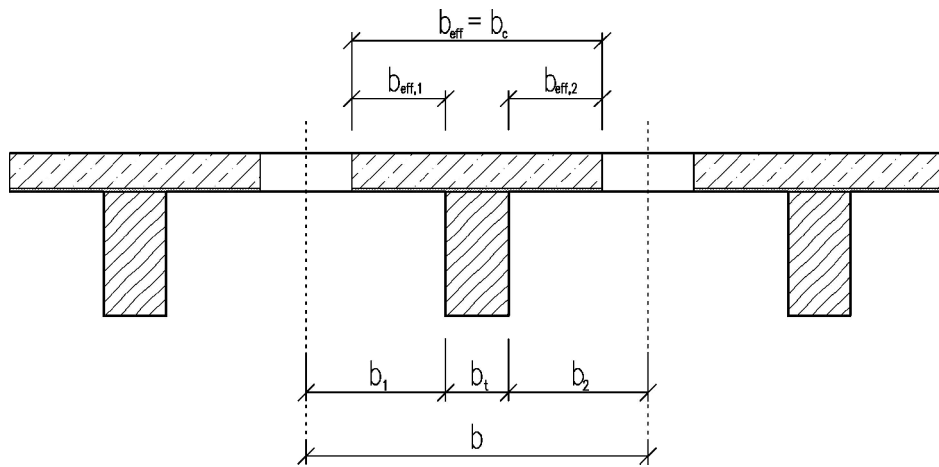


Figure 6.4: Effective flange width

Ratio of moduli of elasticity (stiffness reduction factor) is:

$$n_c = \frac{E_c}{E_t} \quad (6.4)$$

where E_c is a mean modulus of elasticity of concrete and E_t is a mean modulus of elasticity of timber.

Distances from the centre of gravity of concrete layer to the main neutral axis can be obtained according to equation (6.5):

$$z_c = \frac{h_c}{2} + \frac{h_t}{2} - z_t + t_w \quad (6.5)$$

where z_c is a distance from overall neutral axis to the centre of gravity of the concrete layer.

The connection efficiency factor in plane between concrete and timber (γ_{ct}) can be defined using Eurocode 5 in the form of:

$$\gamma_{ct} = \frac{1}{1+p}; \quad p = \frac{\pi^2 \cdot E_{cm} \cdot A_c \cdot s_i}{K \cdot l_{eff}^2} \quad (6.6)$$

where l_{eff} is an effective (buckling) length of the composite beam; A_c is the effective area of concrete slab; s_i is an effective spacing between fasteners and K is a slip modulus taken from Eurocode 5.

For dowel-type fasteners the concrete to timber connections K_{ser} (slip modulus for serviceability) should be based on mean density (ρ_m) of timber member and finally increased (multiplied) by 2,0 which means that connector does not deform in the concrete layer. However, according to experiments performed at the Czech Technical University in Prague, the deformation of connector in concrete always occurs. The stiffness coefficient (also called “connection efficiency factor”) for members glued together (without slip) can be considered $\gamma_{ct} = 1,0$. The final form for K is following:

$$K_{ser} = 2,0 \cdot \frac{\rho_m^{1,5} \cdot d}{23} \quad \text{for serviceability limit state} \quad (6.7)$$

which is valid for dowel-type fasteners (nails with pre-drilling, screws and dowels; for nails without pre-drilling the diameter d should be powered by 0,8.

$$K_u = \frac{2}{3} \cdot K_{ser} \quad \text{for ultimate limit state} \quad (6.8)$$

The effective bending stiffness $(EI_y)_{eff}$ of mechanically jointed elements can be written in the form of:

$$(EI_y)_{eff} = E_c \cdot \left(\frac{h_c^3 \cdot b_c}{12} + \gamma_{ct} \cdot A_c \cdot z_c^2 \right) + E_t \cdot \left(\frac{h_t^3 \cdot b_t}{12} + A_t \cdot z_t^2 \right) \quad (6.9)$$

By using the ratio of moduli of elasticity from equation (6.4) the effective bending stiffness is developed as:

$$E_t \cdot I_{y,eff} = E_t \cdot \left[n_c \cdot \left(\frac{h_c^3 \cdot b_c}{12} + \gamma_{ct} \cdot A_c \cdot z_c^2 \right) + \left(\frac{h_t^3 \cdot b_t}{12} + A_t \cdot z_t^2 \right) \right] \quad (6.10)$$

6.2.2 Determination of Moment Resistance

Normal stresses in the composite section for each subcomponent are determined as follows:

$$\sigma = \frac{M}{W} = \frac{M_y \cdot E_i}{(EI_y)_{eff}} \cdot (\gamma_i \cdot z_i \pm \Delta z) \quad (6.11)$$

where M_y is the belonging bending moment around the appropriate axis (see figure 6.3); Δz is distance from the centre of gravity of the subcomponent to the edge (or any fibre) of the subcomponent; E_i is a modulus of elasticity for appropriate subcomponent.

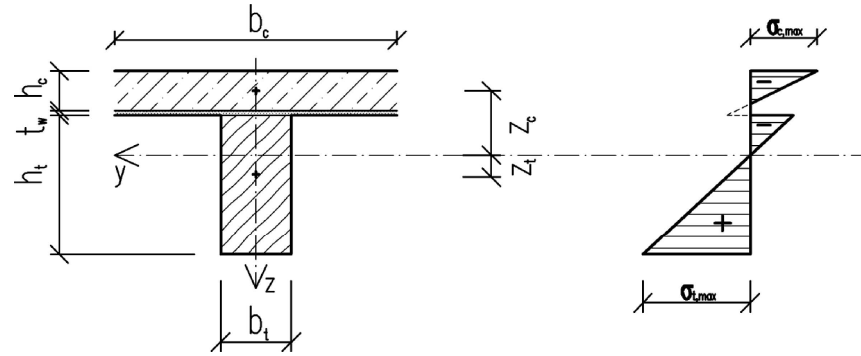


Figure 6.5: Distribution of the normal stress in cross-section

With usage of equation (6.11) and (6.9) normal stresses in the edges of the concrete slab (see figure 6.5) is obtained in the form of:

$$|\sigma_c| = \frac{M_y \cdot n_c}{I_{y,eff}} \cdot \left(\gamma_{ct} \cdot z_c \pm \frac{h_c}{2} \right) \leq f_{c,k} \quad (6.12)$$

where $f_{i,k}$ represents a characteristic strength of a subcomponent material for normal stress. The magnitude of normal stress in the edge fibres of the timber beam is obtained as:

$$\sigma_t = \frac{M_y}{I_{y,eff}} \cdot \left(z_t + \frac{h_t}{2} \right) \leq f_{m,k} \quad (6.13)$$

For normal stresses in the centre of the timber beam (see figure 6.5):

$$\sigma_t = \frac{M_y}{I_{y,eff}} \cdot (z_t) \leq f_{t,0,k} \quad (6.14)$$

According to equations (6.12) to (6.14) a design bending moment resistance can be evaluated:

$$M_{y,Rd} = \sigma_d \cdot W_{y,eff} = f_{i,d} \cdot \frac{I_{y,eff}}{n_i \cdot (\gamma_i \cdot z_i \pm \Delta z)} \quad (6.15)$$

If the concrete slab under compression is decisive, equation (6.16) is obtained:

$$M_{y,Rd,c} = \frac{\alpha}{\gamma_c} \cdot M_{y,Rk,c} = \left(f_{c,k} \cdot \frac{I_{y,eff}}{n_c \cdot \left(\gamma_{ct} \cdot z_c + \frac{h_c}{2} \right)} \right) \quad (6.16)$$

where α is a coefficient taking into account long term effects on the compressive strength and unfavourable effects resulting from the way a load is applied (the value should lie between 0,8 and 1,0 and may be found in the National Annex of Eurocode 2, however, the recommended value is 1,0). γ_c and γ_M are partial safety factors for concrete and timber respectively and may be found in Eurocode.



Figure 6.6: Typical failure of a timber-concrete composite beam: cracking of the timber beam due to tension

If the bending of the timber beam is decisive (which is mostly the case), equation (6.17) gives a relevant moment resistance:

$$M_{y,Rd,t} = \frac{k_{\text{mod}}}{\gamma_M} \cdot M_{y,Rk,t} = \frac{k_{\text{mod}}}{\gamma_M} \cdot \left(f_{m,k} \cdot \frac{I_{y,\text{eff}}}{z_t + \frac{h_t}{2}} \right) \quad (6.17)$$

In cases when the normal stress in the centre of timber beam is high, the equation (6.18) must be used if equation (6.19) is satisfied:

$$M_{y,Rd,t} = \frac{k_{\text{mod}}}{\gamma_M} \cdot M_{y,Rk,t} = \frac{k_{\text{mod}}}{\gamma_M} \cdot \left(f_{t,0,k} \cdot \frac{I_{y,\text{eff}}}{z_t} \right) \quad (6.18)$$

$$1 + \frac{h_t}{2 \cdot z_t} \geq \frac{f_{m,k}}{f_{t,0,k}} \quad (6.19)$$

6.2.3 Determination of Shear Resistance

Shear stress in section for any fibre is given as:

$$\tau = \frac{V \cdot S}{I \cdot b} = \frac{V_z \cdot \sum S_{y,i}^{(y)} \cdot n_i}{I_{y,\text{eff}} \cdot b_i} \quad (6.20)$$

where V_z is shear force in direction of appropriate axis (figure 6.3); $S_{y,i}$ is a first moment of area of section above (or below) investigated fibre in function of subcomponent modulus of elasticity and potential stiffness coefficient (γ_{ct}); b_i is the width of the section at investigated fibre.

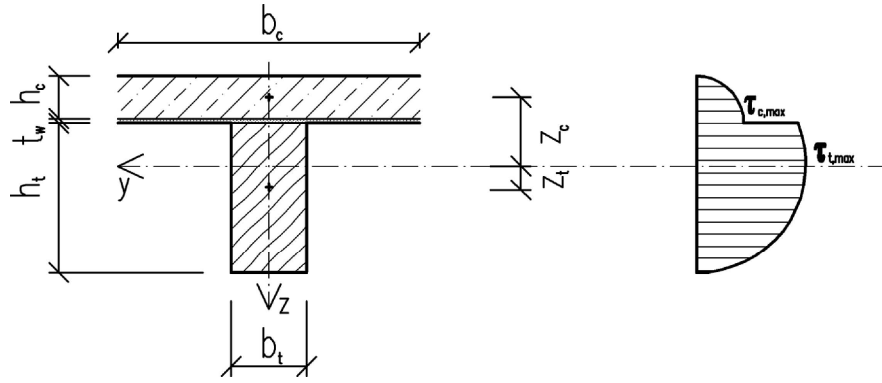


Figure 6.7: Distribution of the shear stress within a cross-section

With usage of equation (6.20), the shear stress in the bottom edge of concrete slab (see figure 6.6) is obtained in form of:

$$\tau_c^{\max} = \frac{V_z \cdot n_c \cdot \gamma_{ct} \cdot h_c \cdot b_c \cdot z_c}{I_{y,eff} \cdot b_c} \leq v_{R,k,1} \quad (6.21)$$

For a determination of the maximal shear stress at neutral axis of the composite cross section (which is in most cases the decisive part of cross-section, regarding the shear stress), the equation (6.22) is used:

$$\tau_t^{\max} = \frac{V_z \cdot \left(n_c \cdot \gamma_{ct} \cdot h_c \cdot b_c \cdot z_c + b_t \cdot \left(\frac{h_t}{2} - z_t \right) \cdot \left(\frac{h_t}{4} - \frac{z_t}{2} \right) \right)}{I_{y,eff} \cdot b_t} \leq f_{v,k} \quad (6.22)$$

where $f_{v,k}$ and $v_{R,k,1}$ present characteristic shear strength of subcomponent material. For concrete according to Eurocode 2, the characteristic shear strength is taken as:

$$v_{R,k,1} = v_{R,k} \cdot k \cdot (1,2 + 40 \cdot \rho_l); \quad k = (1,6 - d) \quad (6.23)$$

where $v_{R,k}$ presents basic characteristic shear strength of concrete from; d is a static height of a concrete slab in metres and ρ_l is a longitudinal reinforcement percentage.

According to equations (6.21) and (6.22), the design shear force resistance can be evaluated as:

$$V_{z,Rd,i} = \frac{I_{y,eff} \cdot b_i}{f_{i,d} \cdot \sum S_{y,i}^{(y)} \cdot n_i} \quad (6.24)$$

If the shear stress in concrete is decisive (which is not usual), equation (6.25) is obtained:

$$V_{z,Rd,c} = \frac{1}{\gamma_c} \cdot V_{z,Rk,c} = \frac{1}{\gamma_c} \cdot \left(v_{R,k,1} \cdot \frac{I_{y,eff} \cdot b_c}{n_c \cdot \gamma_{ct} \cdot h_c \cdot b_c \cdot z_c} \right) \quad (6.25)$$

However, in most cases, the shear resistance of timber beam is decisive. In that case equation (6.26) is obtained:

$$V_{z,Rd,t} = \frac{k_{mod}}{\gamma_M} \cdot V_{z,Rk,t} = \frac{k_{mod}}{\gamma_M} \cdot \left[f_{v,k} \cdot \frac{I_{y,eff} \cdot b_t}{n_c \cdot \gamma_{ct} \cdot h_c \cdot b_c \cdot z_c + b_t \cdot \left(\frac{h_t}{2} - z_t \right) \cdot \left(\frac{h_t}{4} - \frac{z_t}{2} \right)} \right] \quad (6.26)$$

6.2.4 Determination of Fastener Bearing Capacity

Force on one fastener from equation (6.20) in function of distance between fasteners (s_i) is given as:

$$F_i = \frac{V_z \cdot S_i \cdot E_i}{(EI_y)_{eff}} \cdot s_i = \frac{V_z \cdot \sum S_{y,i}^{(y)} \cdot n_i}{I_{y,eff}} \cdot s_i \quad (6.27)$$

Attention must be also paid to the minimal intervals (spacing of fasteners), edge and end distances for different type of fasteners. In the case illustrated in figure 6.8, equation (6.28) must be satisfied.

$$F_{v,Ed} = \frac{V_{z,d} \cdot n_c \cdot \gamma_{ct} \cdot h_c \cdot b_c \cdot z_c}{I_{y,eff}} \cdot s_i \leq F_{v,Rd} \quad (6.28)$$

Consequently design shear resistance may be expressed as:

$$V_{z,Rd,f} = \frac{k_{mod}}{\gamma_M} \cdot V_{z,Rk,f} = \frac{k_{mod}}{\gamma_M} \cdot \left[F_{v,Rk} \cdot \frac{I_{y,eff}}{n_c \cdot \gamma_{ct} \cdot h_c \cdot b_c \cdot z_c \cdot s_i} \right] \quad (6.29)$$

where the force $F_{v,Rk}$ is a characteristic load carrying capacity per shear plane per fastener. Values of $F_{v,Rk}$ for individual fasteners can be calculated according to Eurocode 5 part 1-1 and their load-carrying capacity according to the modified Johansen yield theory (Eurocode 5, part 2). Load-carrying capacity of some fasteners must be determined by experiments.

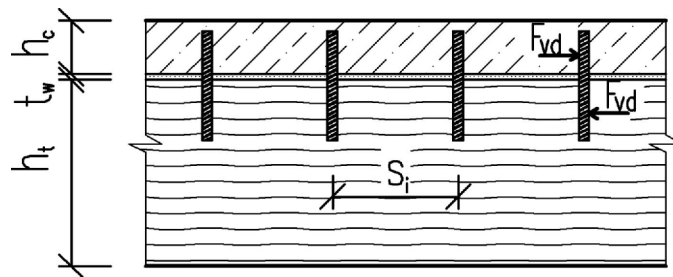


Figure 6.8: Fasteners and forces acting on them

Fasteners in connection are commonly spaced according to the shear force in the interface, and in this case an effective constant spacing s_{eff} is assumed for the calculation of γ_{ct} :

$$s_{eff} = 0,75 \cdot s_e + 0,25 \cdot s_m \quad (6.30)$$

with $s_e < s_m < 4s_e$ where s_e is the spacing at the ends of the beam and s_m is the spacing in the middle.

6.3 Comparison of Results with Laboratory Tests and Numerical Models

Above described procedure was used for the development of Excel spreadsheet enabling fast calculation of load-bearing capacity and deflection. The results given by this calculation were compared with results of laboratory tests, carried out at the ETH Zurich.

Detailed experimental results of the laboratory tests performed at the ETH are described in *Versuche zum Tragverhalten von Holz-Beton-Verbunddecken bei Raumtemperatur und Normbrandbedingungen* by Frangi and Fontana from July 2000.

The shear connection consists of 20 mm deep and 150 mm long grooves, reinforced with steel dowels (threaded bars M12) fixed in a 80 mm deep hole in the timber member with a special glue. The geometry is described in figure 6.9, slip modulus was experimentally measured.

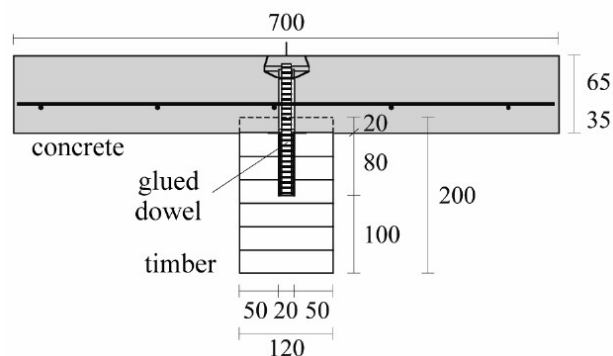


Figure 6.9: Cross-section of the timber-concrete composite beams with grooved connections

The timber beams consisted of glued laminated timber beams of spruce with a density between 420 and 478 kg/m³. All specimens had a moisture content of $12 \pm 1\%$. The E-modulus of the timber beams was obtained from bending tests before the concrete slab was poured.

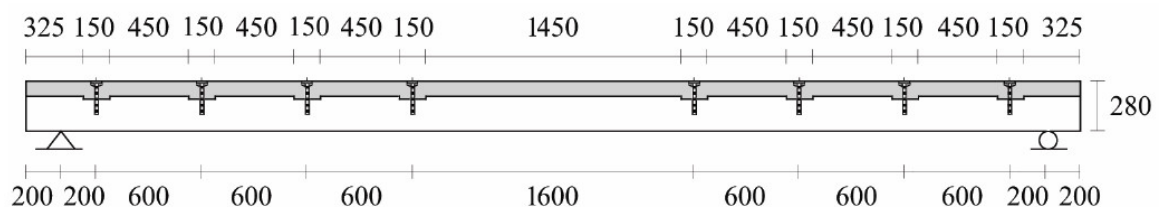


Figure 6.10: Longitudinal-section of the timber-concrete composite beam with grooved connections and glued steel dowels used for bending tests

A series of four-point short-term bending tests as shown on figure 6.11 observed the structural behaviour of the timber-concrete composite members with grooved connections and

glued steel dowels. The span of the simply supported beams was 5,6 m, the spacing between support and the point load was 1,8 m.

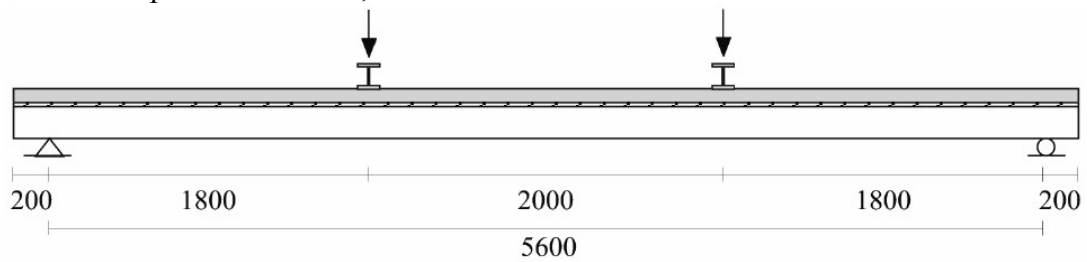


Figure 6.11: Static system for the four-point short-term bending tests

The timber-concrete composite beams showed linear-elastic behaviour up to about 25 kN. In this load range very small slip deformations were measured. This confirms the high slip stiffness of the grooved connection with glued steel dowels. By increasing the load level, a non-linear behaviour of the timber-concrete composite beams due to the non-linear increase of the slip deformations was observed.

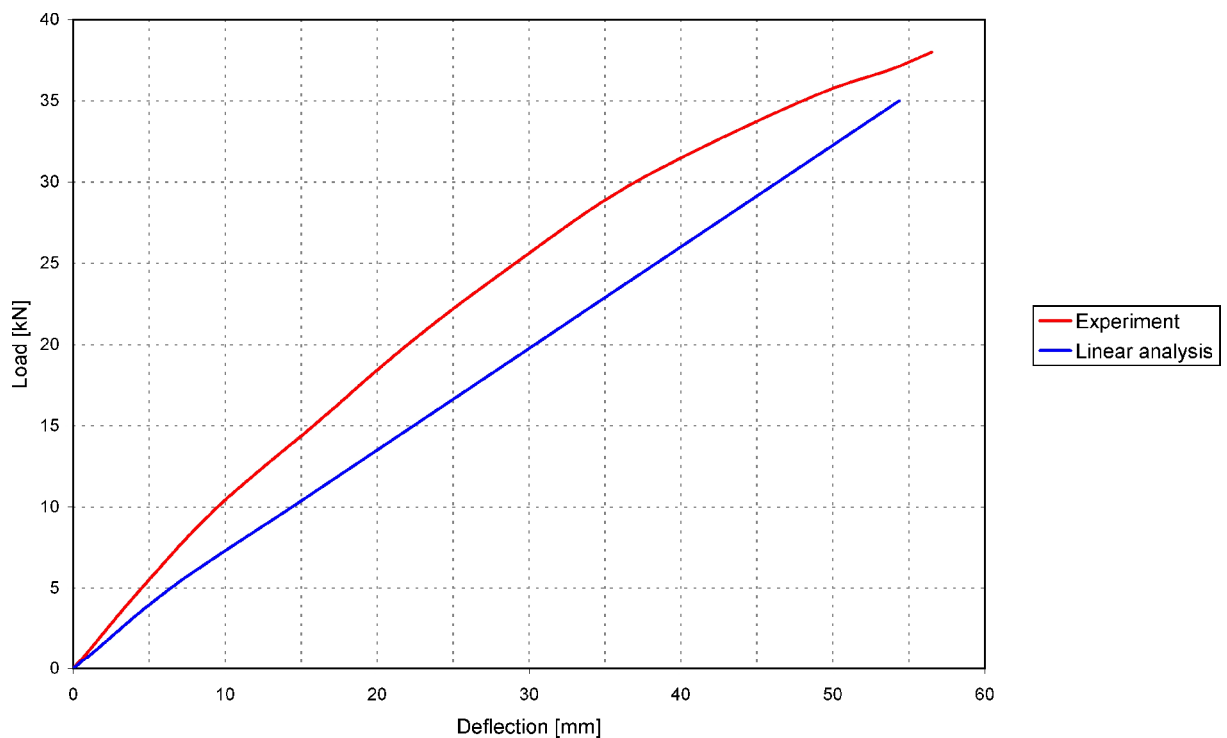


Figure 6.12: Comparison of results of analytical calculation with results from experiments

The figure 6.12 shows that calculated deflection is higher than in reality; however with an increasing load the curves are getting closer. This is due to the fact, that the slip modulus used for the linear calculation is approximated as a secant of the F-u diagram (see figure 6.2) and does not reflect the real behaviour of the connection. The tested beam collapsed due to tensile cracking of timber beam as predicted by the linear analysis. The predicted load-level at collapse was 35 kN, during the experiments the maximum load reached was 38 kN.

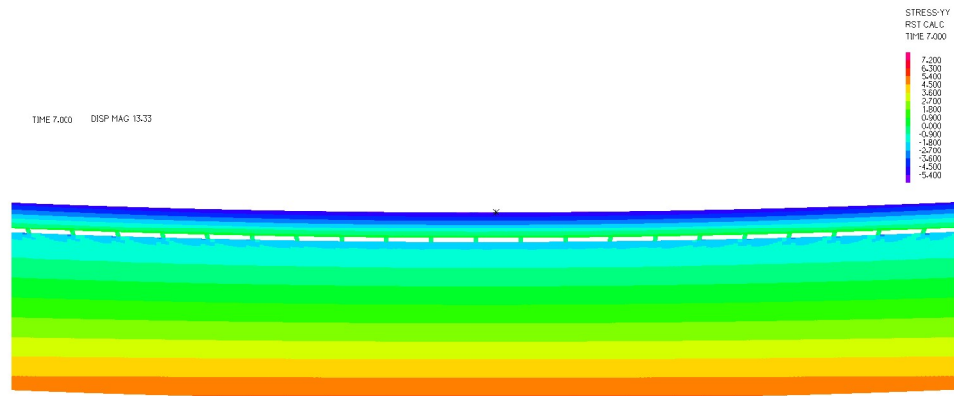


Figure 6.13: Distribution of normal stress in beam at midspan

The numerical model executed in ADINA Structures software, calculating with non-linear behaviour of concrete and linear behaviour of timber and connectors gave very similar results to those from linear analysis. For an exact modelling, non-linearity of all components would have to be taken into account, since even behaviour of timber is viscoelastic.

For investigation of long-term effects, the model should take into account creep of concrete and timber.

6.4 Serviceability Limit State

Average values of moduli are used to calculate instantaneous (elastic) deflection. For vibration calculations an increase of 10% in moduli is appropriate. When calculating long-term performance, simplifying assumptions can be adopted to account for creep phenomena, i.e. by taking reduced stiffness values for individual parts.

It may seem that using reduced stiffness properties is a very crude approach to predict long-term deflection of composite systems. However, the experimental evidence is that deformation tends to stabilize after a few years under quasi-permanent design loads. Therefore, the correct final deformation values can be predicted by adopting these approaches.

6.4.1 Instantaneous Bending Stiffness ($t = 0$)

The equations (6.4) and (6.5) remain the same; equations (6.1), (6.8), (6.9) and (6.10) are modified by γ_{ct} where usage of K_{ser} instead of K_u makes the only difference in equation (6.6). All the partial safety factors equal to 1,0 and calculations should be performed with characteristic values for loading.

6.4.2 Long-Term Bending Stiffness ($t = \infty$)

The time dependent effects (creep) can be associated with the modulus of elasticity of material of each subcomponent. In equation (6.4) the modified, so called effective moduli of elasticity according to Eurocode 5 and Eurocode 2, are used in form of:

$$E_{mean,fin} = \frac{E_{mean}}{1 + \psi_2 \cdot k_{def}} \quad \text{for timber subcomponent} \quad (6.31)$$

$$E_{c,eff} = \frac{E_c}{1 + \varphi_{(\infty, t_0)}} \quad \text{for concrete subcomponent} \quad (6.32)$$

where k_{def} presents the final creep coefficient for individual service classes given by Eurocode 5. The factor ψ_2 is given by Eurocode 1 and takes into account the duration of individual loads. Regarding the creep of concrete, the creep coefficient is calculated according to the model in Eurocode 2 (based on Rüsç model) and depends on relative humidity of ambient environment and predicted loading.

Time dependent effects on connection are associated with change of modulus K_{ser} by modification according to equation from Eurocode 5:

$$K_{ser,fin} = \frac{K_{ser}}{1 + \left(\frac{\psi_2 \cdot k_{def} + \varphi_{(\infty, t_0)}}{2} \right)} \quad (6.33)$$

Above mentioned modifications of individual moduli have direct influence on stiffness coefficient (γ_{ct}) in equation (6.6) and consequently on equation (6.1) and on bending stiffness given in equations (6.8), (6.9) and (6.10).

There is still some uncertainty about suitable modelling of time-dependent effects on composite action. However, the influence of creep in ultimate limit state (ULS) calculations must not be neglected in case of such composed sections. The creep has a big influence on redistribution of stresses in section, especially when cross-section is composed of different creep suffering materials.

According to Kavaliauskas (2005) the stresses in a concrete part of the composite cross-section significantly decrease in time (from 1,4 to 5 times) while it slightly increases in timber part (approximately 2 times). Also creep effects in connection between timber and concrete part of the section have a significant influence on the distribution of stresses.

From that can be concluded that the rheological phenomena (creep) of connection in calculation of deformation – serviceability limit state and also in the calculation of bearing capacity of an element section – ultimate limit state must be taken into account. In above described calculation procedure, a creep effects present in connection are taken into account through final slip modulus $K_{ser,fin}$.

7 Fire Design of Timber-Concrete Composite Floors

The knowledge of a fire behaviour of the timber-concrete composite beam and used mechanical connection is necessary to achieve a reliable and economic design of this construction in case of fire. Fire research carried out by Fontana and Frangi (Frangi 2000) shows that the timber-concrete composite beam can be designed according to γ -method with charring of the timber part of the composite structure specified by the charring rate β and the stiffness reduction due to elevated temperature of the shear connection k_{mod} . Also concrete is deteriorating with an increasing temperature and thus its load-bearing capacity and stiffness is significantly reduced.

There have been studies investigating the behaviour of timber-concrete composites arising from different thermal expansion of individual components and temperature gradient within the cross-section. All studies have proven that the effect of different thermal expansion and temperature gradient is small and can be neglected.

All the following calculations are based on ISO 834 fire exposure. The criteria for floor structures are load-bearing capacity (R) which is being checked by the proposed calculation procedure, integrity (E) which is in fact automatically fulfilled together with the criterion for load-bearing capacity, and finally the insulation function (I) which should be checked if required.

Critical deflection and rates of deflection are normally given as criteria for load-bearing capacity. The integrity is generally evaluated by means of the development of gaps of excessive size that are compared with a maximal allowed size given by national codes. The criterion for insulation is fulfilled if the mean temperature rise of 140°C or maximal temperature rise of 180°C is not exceeded.

According to Czech Standards following classes of load-bearing capacity criterion are evaluated (for columns, beams and bracings): R 15, R 30, R 45, R 60, R 90, R 120, R 180

7.1 Mechanical Loading During Fire

The following procedure is based upon the verification of resistance of structure weakened by fire against the effect of reduced loading in a fire situation:

$$R_{fi,d,t} \leq E_{fi,d,t} \quad (7.1)$$

where $R_{fi,d,t}$ is the design value of the resistance of the member in the fire situation at time t and $E_{fi,d,t}$ is the design value of the relevant effects of actions in the fire situation at time t .

For obtaining the relevant effects of actions $E_{fi,d,t}$ during fire exposure, the mechanical actions shall be combined in accordance with EN 1990 "Basis of structural design" for accidental design situations.

The representative value of the variable action Q_I may be considered as the quasi-permanent value $\psi_{2,1} \cdot Q_I$, or in case of halls where snow and wind load have a significant effect on the structure $\psi_{1,1} \cdot Q_I$ should be used instead of quasi-permanent value.

The effect of actions should be determined for time $t = 0$ using combination factors $\psi_{1,1}$ or $\psi_{1,2}$ according to EN 1991-1-2 Section 4. As a simplification the effects of actions may be obtained from a structural analysis for normal temperature design as:

$$E_{d,fi} = \eta_{fi} \cdot E_d \quad (7.2)$$

where E_d is the design value of the corresponding force or moment for normal temperature design for a fundamental combination of actions and η_{fi} is the reduction factor for the design load level for the fire situation.

The reduction factor η_{fi} for basic load combination (for complicated load combinations see EN 1990) should be taken as:

$$\eta_{fi} = \frac{E_{fi,d}}{E_d} = \frac{G_k + \psi_{Q,1} \cdot Q_{k,1}}{\gamma_G \cdot G_k + \gamma_{Q,1} \cdot Q_{k,1}} \quad (7.3)$$

Generally structures with a low self-weight have smaller value of the reduction factor and therefore higher fire resistance. For simplifications the reduction factor may be used as 0,65 (with exception of storage areas) for timber structures and 0,7 for concrete structures. However, these values are rather conservative.

7.2 Nominal Temperature-Time Curves

The nominal or standard fire curves are the simplest way to represent a fire by pre-defining some arbitrary temperature-time relationship, which are independent on ventilation and boundary conditions. Historically, they were developed for fire resistance furnace tests of building materials and elements for their classification and verification.

The main disadvantage and limitation of standard fires is that they do not represent real natural fire. The differences in the heating rate, fire intensity and duration between the standard and real fires can result in different structural behaviour. For example, a short duration high temperature fire can result in spalling of concrete exposing steel reinforcement due to the thermal shock.

Even though there are above mentioned disadvantages and limitations of nominal curves, design performance-based approaches have been developed based on the results and observations from a standard fire resistance tests.

According to fuel type and ventilation conditions, EC provides designers with different standard curves e.g. for external fire (for the outside of external walls which can be exposed to fire from different parts of the facade), standard fire (representing a fully developed compartment fire) and hydrocarbon fire (representing a fire with hydrocarbon or fuel of liquid type). EN 1991-1-2 provides three nominal fire curves as follows:

a) for standard fire:

$$\theta_g = 20 + 345 \log_{10}(8t + 1) \quad (7.4)$$

b) for external fire:

$$\theta_g = 20 + 660 \left(1 - 0,687e^{0,32t} - 0,313e^{0,38t} \right) \quad (7.5)$$

c) for hydrocarbon fire:

$$\theta_g = 20 + 1080 \left(1 - 0,325e^{-0,167t} - 0,675e^{-2,5t} \right) \quad (7.6)$$

d) for a slow fire development in cavities (e.g. soffits, double floors) nominal curve:

$$\theta_g = 20 + 154\sqrt[4]{t} \quad (7.7)$$

can be used until the 20th minute of fire, followed by:

$$\theta_g = 20 + 345 \log_{10} [8(t - 20) + 1] \quad (7.8)$$

that is applicable until the 40th minute of fire. In equations (7.4) to (7.8) θ_g is the gas temperature in the fire compartment or near the member in °C and t is the time in minutes.

There are many advanced fire models (one zone, two zone, computational fluid mechanics) giving more accurate results than nominal curves. However, these advanced models are not easy to use and thus for the simplified calculation designers tend to use above mentioned nominal curves.

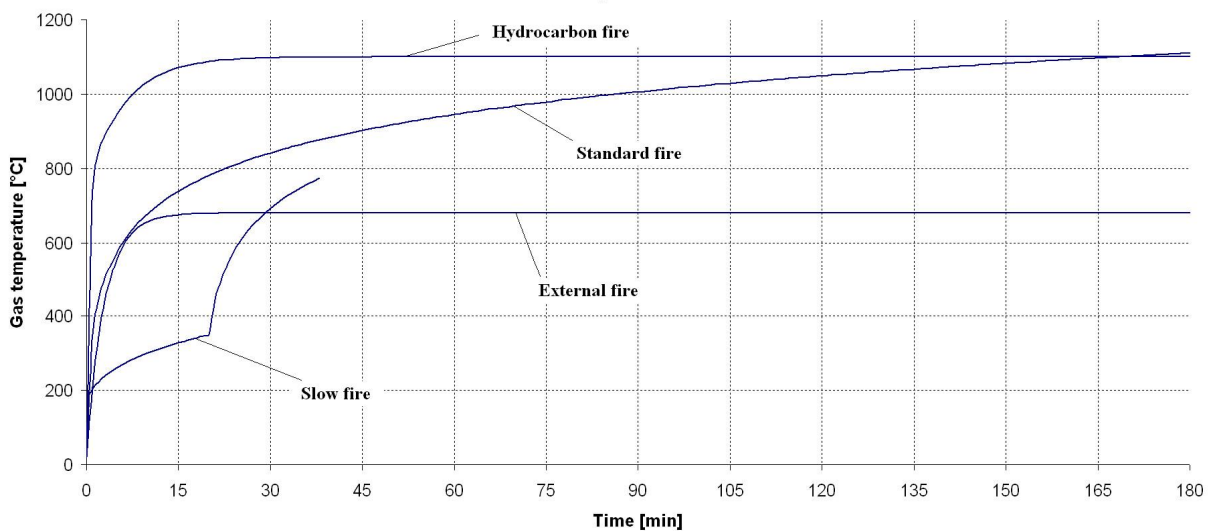


Figure 7.1: Nominal temperature-time curves

7.3 Behaviour of Timber in Fire

Timber is a combustible material and therefore differs from most other commonly used structural building materials. When sufficient heat is applied to wood, a process of thermal degradation (pyrolysis) takes place producing combustible gases, accompanied by a loss in mass. A charred layer is then formed on the fire-exposed surfaces and the char layer grows in thickness as the fire progresses, reducing the cross-sectional dimensions of the timber member. The char layer as a good insulator protects the remaining uncharred residual cross section against heat.

The process of thermal degradation starts when the temperature of wood reaches a certain threshold value which depends on a kind of wood, but is generally around 300°C. Because of the importance and complexity of the pyrolysis of timber, there is a substantial volume of work on the pyrolysis and charring of timber as a porous medium. Experimental observations of charring behaviour prove the mutual effect of temperature and moisture content gradients in timber, but it is rarely taken into consideration in the computational analysis of charring in fire situations.

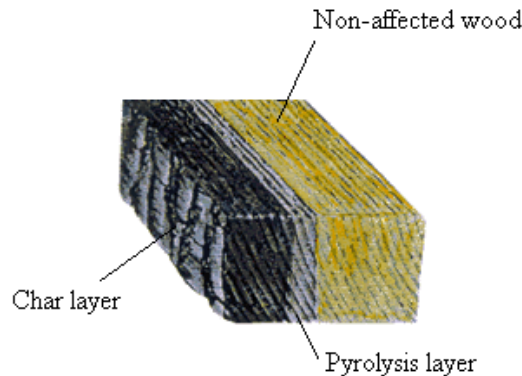


Figure 7.2: Deterioration of wood during the burning process

There have been many models developed in past years (Shaffer's, Lawson's etc.) and these models differ slightly at the beginning, but are virtually equal at 60min. Similarly, the model proposed by Eurocode 5. Most of the models are relatively simple to use. However, all empirical models are limited to one-dimensional cases. In all empirical models it is assumed also that charring of timber starts instantaneously after the exposure to fire. In reality, this is not the case, because charring starts when the temperature of timber reaches the temperature of pyrolysis, which is around 300°C. In this case, this happens usually around 4 minutes after the fire starts.

The boundary between the timber and the char is defined as a temperature isotherm of 300°C. It can be seen that temperature gradients are the highest at the boundary between the timber and the char. Charring is the fastest at the beginning and due to the material properties of the char, it gradually decreases with time. Since corners are subjected to heat and moisture transfer from two directions, charring is faster at corners. As a result, a rounding effect occurs and shortly after the ignition the remaining load-bearing cross-section is no longer rectangular.

For exact calculation, a transient heat and moisture transfer over a timber beam exposed to standard fire conditions is considered. The governing equations of simultaneous heat and moisture transfer in porous media like timber were provided by Luikov.

7.3.1 Basic Assumptions and Determinations for Calculation

Results of many tests for wood and wood-based materials have shown a linear relationship between charring depth and time. A constant charring rate can be therefore assumed for calculation of the fire resistance of a section. Charring rates given by Eurocode 5 can be used for simple methods of structural fire design without need to take any special consideration of the rounding of edges. Therefore the residual cross-section is considered to be rectangular in fire design calculations.

The charring rate of a timber beam is taken from Eurocode 5 as β_n taking into account rounding effect and fissures. Then the charring depth d_{char} reducing the effective cross-section is calculated as:

$$d_{char} = \beta_n \cdot t \quad (7.9)$$

where t is time of fire exposure in minutes and β_n equals 0,8 for solid softwood with density $\geq 290 \text{ kg/m}^3$, 0,7 for softwood glulam timber with a characteristic density $\geq 290 \text{ kg/m}^3$ and

hardwood solid or glulam timber with a characteristic density $\geq 290 \text{ kg/m}^3$. For hardwood with characteristic density $\geq 450 \text{ kg/m}^3$ β_n may be considered as 0,55 and 0,7 for LVL with characteristic density $\geq 450 \text{ kg/m}^3$.

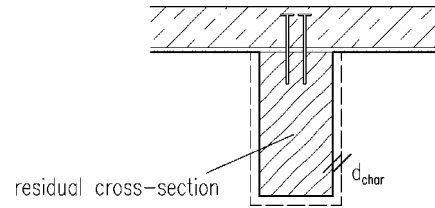


Figure 7.3: Residual cross-section

The design values of strength and stiffness of residual cross-section are:

$$f_{fi,d} = k_{mod,fi} \cdot k_{fi} \cdot \frac{f_k}{\gamma_{M,fi}} \quad \text{for strength characteristics} \quad (7.10)$$

$$E_{fi,d} = k_{mod,fi} \cdot k_{fi} \cdot \frac{E_{k,05}}{\gamma_{M,fi}} \quad \text{for stiffness} \quad (7.11)$$

$$E_{fi,d} = k_{mod,fi} \cdot \frac{E_{mean}}{\gamma_{M,fi}} \quad \text{for calculation of deflection} \quad (7.12)$$

where $k_{mod,fi}$ is the modification factor for fire, taking into account the influence of temperature and moisture on the parameters of strength and stiffness of material; k_{fi} converts characteristic value on the 20% fractile value ($k_{fi} = 1,25$ for solid timber and 1,15 for glulam); $\gamma_{M,fi}$ is partial safety factor ($\gamma_{M,fi} = 1,0$); f_k is a characteristic strength at room temperature; $E_{k,05}$ is a characteristic value of modulus of elasticity for 5% fractile at room temperature, while E_{mean} is an average value of modulus of elasticity at room temperature.

Using reduced properties method, $k_{mod,fi}$ is determined as:

$$k_{mod,fi} = 1,00 - \frac{p}{200A_r} \quad \text{for bending strength} \quad (7.13)$$

where p is a perimeter of residual cross-section exposed to fire in metres; A_r is an area of residual cross-section in square metres.

7.4 Behaviour of Shear Connectors at Elevated Temperature

The structural behaviour of timber-concrete composite slabs is mainly governed by the shear connection between timber and concrete. When a timber-concrete composite structure is exposed to fire, it is of particular importance to know the changes in stiffness and strength that shear connection is subjected to.

The development of temperature inside the beam is highly dependent on the timber beam width. The calculations are based on the study of the width effect under nominal fire exposure

carried out by Frangi, Knobloch and Fontana from the Institute of Structural Engineering in Zurich. During these experiments the temperature inside the timber beam were measured.

Based on results from experiments, Frangi, Knobloch and Fontana developed formulas for reduction factors for the slip modulus and also for the strength of screwed connections. However, in proposed calculation, these reduction factors are used also for other types of connectors. For more accurate determination of reduction factors of other connectors, numerical models and experiments have to be performed.

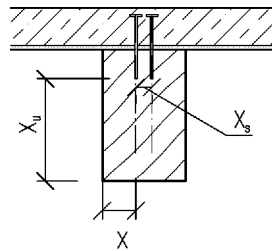


Figure 7.4: Determination of timber side cover x

The fire tests showed that the temperature measured around the connection mainly depends on the timber side cover x (see figure 7.4) of the connection. Therefore, using the temperature profile and a temperature-dependent reduction of connectors according to Frangi, Knobloch and Fontana, simplified relationships for strength and stiffness of the connection depending on the position of the connectors in the timber beams (i.e. timber side cover) were obtained. In this way the temperature in the timber beam does not need to be determined, making the calculation of the strength and stiffness properties of the screwed connection in fire much easier for the designer.

The temperature-dependent reduction of stiffness and strength of the screwed connection is considered using the modification factors $k_{mod,fi}$. The modification factors $k_{mod,fi}$ of the screwed connection depend on the side cover x of the connectors. The influence of the heat flux from the bottom and the opposite side of the connector may be neglected if $x_u \geq x + 20$ mm and $x_s \geq 20$ mm. The following formulas were developed:

a) reduction factors of the slip modulus of connectors:

$$\begin{aligned}
 k_{mod,fi} &= 0 & \text{for} & & x \leq 0,6t \\
 k_{mod,fi} &= \frac{0,2x - 0,12t}{0,2t + 3} & \text{for} & & 0,6t \leq x \leq 0,8t + 3 \\
 k_{mod,fi} &= \frac{0,8x - 0,6t + 1,8}{0,2t + 21} & \text{for} & & 0,8t + 3 \leq x \leq t + 24 \\
 k_{mod,fi} &= 1,0 & \text{for} & & x \geq t + 24
 \end{aligned} \tag{7.14}$$

b) reduction factors for the strength of connectors:

$$\begin{aligned}
 k_{\text{mod},fi} &= 0 & \text{for} & \quad x \leq 0,6t \\
 k_{\text{mod},fi} &= \frac{0,44x - 0,264t}{0,2t + 5} & \text{for} & \quad 0,6t \leq x \leq 0,8t + 5 \\
 k_{\text{mod},fi} &= \frac{0,56x - 0,36t + 7,32}{0,2t + 23} & \text{for} & \quad 0,8t + 5 \leq x \leq t + 28 \\
 k_{\text{mod},fi} &= 1,0 & \text{for} & \quad x \geq t + 28
 \end{aligned} \tag{7.15}$$

where x is a side cover in mm as shown in figure 7.4; t is a fire duration in minutes. Above mentioned reduction factors are used for the reduction of stiffness of the shear connection, where partially plastic deformation of the connector is allowed (and therefore K_{ser} is being used):

$$K_{fi} = k_{\text{mod},fi} \cdot K_{ser} \tag{7.16}$$

The ultimate limit state in fire for the design load $F_{v,Ed,fi}$ on the connector can be verified as follows:

$$F_{v,Ed,fi} \leq F_{v,Rd,fi} = k_{\text{mod},fi} \cdot k_{fi} \cdot F_{v,Rk} \tag{7.17}$$

However, the failure of connectors does not mean, that the structure has to inevitably fail. If the connection fails, the both components (i.e. concrete and timber) do not cooperate any more and have to carry the load independently and the load-bearing capacity is reduced. In such situation the γ_{ct} coefficient equals to zero.

7.5 Behaviour of Concrete at Elevated Temperature

Concrete does not burn like timber and it does not emit any toxic fumes when affected by fire. It will also not produce smoke or drip molten particles, unlike some plastics and metals, so it does not add to the fire load. For these reasons concrete is said to have a high degree of fire resistance and, in the majority of applications, concrete can be described as virtually “fireproof”. This excellent performance is mainly due to poor thermal conductivity and non-combustibility. It is slow rate of heat transfer that enables concrete to act as an effective fire shield not only between adjacent spaces, but also to protect itself from fire damage.

However, when concrete is exposed to the high temperatures in fire, a number of physical and chemical changes can take place. When the temperature of the surface is higher than 200°C, spalling of concrete usually takes place. It means that pieces of concrete are breaking away from the surface.

With rising temperatures also strength and stiffness of concrete is reduced. In the following sections only normal-weight concrete with siliceous aggregates will be discussed. Data for other types of concrete can be found in Eurocode 2 and calculations performed analogically according to the proposed procedure.

7.5.1 Determination of Temperature within Concrete Layer

Material properties of concrete are strongly dependent on the temperature of the material. To get accurate load-bearing resistance of a structure, temperature development within a

cross-section must be analyzed. For simplified calculations the influence of timber beam is neglected, which provides significantly simpler procedure for designers on the safe side. However interlayer must be taken into account, since its importance is far from negligible. If there is any flooring, it should be also considered in the calculation.

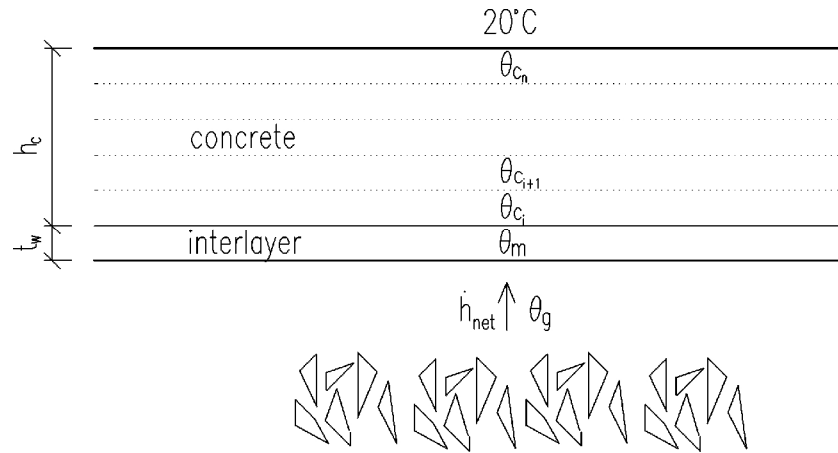


Figure 7.5: Heat flux into the structure

There is always transfer of energy from the fire to surrounding surfaces. This transfer happens via heat flux. The heat flux is composed of convection and radiation. Convective heat flux $h_{net,c}$ depends on the difference in temperatures of emitting body θ_r and heat receiving body θ_m . The rate of energy intake also depends on emissivity coefficient ε_m of receiving surface and on the situation factor Φ (which is for surfaces directly exposed to fire = 1,0). The radiative heat flux is expressed as:

$$h_{net,r} = \Phi \cdot \varepsilon_m \cdot \sigma \cdot [(\theta_r + 273)^4 - (\theta_m + 273)^4] \quad (7.18)$$

resulting in $W \cdot m^{-2}$; $\sigma = 5,6703 \cdot 10^{-8} W \cdot m^{-2} \cdot K^{-4}$ is Stefan-Boltzmann constant. Emissivity coefficients for carbon (char) $\varepsilon_m = 0,77$, for concrete $\varepsilon_m = 0,85$ and for wood $\varepsilon_m \approx 0,9$.

The second component of the total heat flux h_{net} depends is the convective heat flux $h_{net,c}$ depending on the difference in temperature of gas in the vicinity of the heated surface θ_g and temperature of the heated surface θ_m . The convective heat flux is expressed as:

$$h_{net,c} = \alpha_c \cdot (\theta_g - \theta_m) \quad (7.19)$$

resulting in $W \cdot m^{-2}$; α_c is the convective heat transfer coefficient in $W \cdot m^{-2} \cdot K^{-1}$. On the side of concrete layer exposed to fire $\alpha_c = 25 W \cdot m^{-2} \cdot K^{-1}$ for standard and external fire nominal curves. For hydrocarbon fire curve $\alpha_c = 50 W \cdot m^{-2} \cdot K^{-1}$. On the opposite side of the concrete layer $\alpha_c = 9 W \cdot m^{-2} \cdot K^{-1}$ taking into account also the effects of radiation.

As soon as the heat reaches the surface of the body, it begins to spread via conduction through the material (see figure 7.6). This phenomenon is described by Fourier's law as:

$$Q = \lambda \cdot A \cdot \frac{\Delta\theta}{s} \quad (7.20)$$

where Q is the energy intake (heat flux) in watts into the layer of thickness s ; λ is the thermal conductivity coefficient of the material and $\Delta\theta$ is the difference of temperatures of investigated and neighbouring layer. The thermal conductivity coefficient of concrete is changing with temperature: $\lambda = 1,85 - 0,002 \cdot \theta + 8,33 \cdot 10^{-7} \cdot \theta^2 \text{ W} \cdot \text{m}^{-1} \cdot \text{K}^{-1}$, for wood across the grain $\lambda \approx 0,14 \text{ W} \cdot \text{m}^{-1} \cdot \text{K}^{-1}$, for hardwoods $\lambda \approx 0,17 \text{ W} \cdot \text{m}^{-1} \cdot \text{K}^{-1}$.

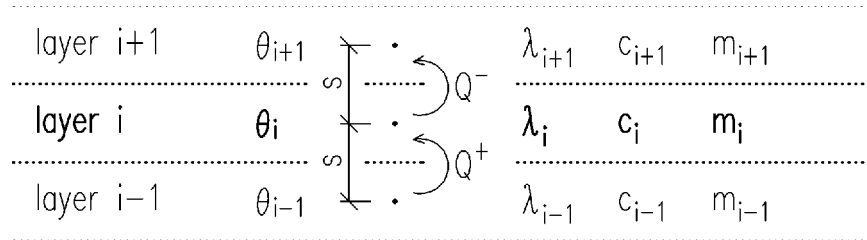


Figure 7.6: Heat conduction within the material

Energy coming into the investigated layer is then converted into the change of temperature of this layer $\Delta\theta$:

$$\Delta\theta = \frac{Q}{c \cdot m} \tag{7.21}$$

where Q is the heat intake (can be also outflow if negative); c is the specific heat capacity of material, for concrete the specific heat capacity is changing with temperature of the material: $c = 900 + 0,667 \cdot \theta + 2,78 \cdot 10^{-4} \cdot \theta^2 \text{ J} \cdot \text{kg}^{-1} \cdot \text{K}^{-1}$; m is the mass of investigated layer in kg with volume $V = A \cdot s$ and density $\rho = 2400 \text{ kg} \cdot \text{m}^{-3}$ for concrete.

For simplified calculation the layer of concrete should be divided into reasonably thin layers and temperatures in each layer should be iteratively calculated. Since fire causes the heat conduction to be transient, incremental method should be employed with the change of boundary conditions (temperature of gas) according to prescribed curves, e.g. nominal ones.

To simplify the procedure as much as possible with reasonably accurate results, formula for temperature within the timber exposed to fire from one side developed by Frangi, Knobloch and Fontana may be used:

$$\theta(x) = \max \left\{ \begin{array}{l} 20 + 180 \left(\frac{\beta_0 \cdot t}{x} \right)^\alpha \\ \theta_g \end{array} \right\} \tag{7.22}$$

where β_0 is a charring rate in mm/min (0,8 for solid softwood with density $\geq 290 \text{ kg/m}^3$, 0,7 for softwood glulam timber with a characteristic density $\geq 290 \text{ kg/m}^3$); t is time in minutes, x is the distance in mm from the original surface exposed to fire and α is calculated as:

$$\alpha = 0,0025t + 1,75 \tag{7.23}$$

By this approach it is not necessary to calculate temperatures within the timber interlayer (if interlayer made of timber is present), but only temperatures within the concrete slab. By this approach, equations (7.18) and (7.19) are avoided in the analysis and only heat conduction in concrete must be calculated. However, if the interlayer is not present, the

equations (7.18) and (7.19) have to be used, because the concrete is directly exposed to radiation and convection.

The maximum function in equation (7.22) ensures that the temperature will not grow higher than temperature of gasses (which is physically not possible) after the interlayer is burnt out.

7.5.2 Cross-Section Temperature According to Analytical and Numerical Model

The above mentioned procedure has been used for the analysis of cross-section with geometry according to figure 7.7 and compared with a numerical analysis performed on the same input data (geometry of cross-section, development of temperature in the compartment, emissivity of materials, convective heat transfer coefficient, conductivity, specific mass and specific heat capacity of materials). The development of temperature in the fire-compartment was considered according to the nominal standard-fire curve. Heating of the space above the floor was taken into account in both models. The surface of the concrete slab was considered without any flooring or any other insulating layer in both calculations. However, thicker layer of flooring with good thermal insulation properties could help to reduce the temperature on the surface of the floor, but on the other hand it could contribute to excessive accumulation of heat in the concrete layer, resulting in reduced strength and stiffness.

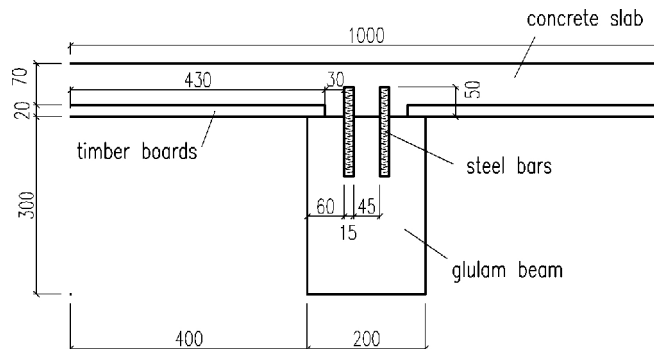


Figure 7.7: Cross-section used for analysis

In the finite element model, the interlayer decking was considered to be combustible as well as timber beam. The pyrolysis process (burning) started at temperature over 300°C and thin layer of charcoal was assumed to create, having a different emissivity, density, thermal capacity and conductivity than original wooden surface of the beam and decking. Moisture movement was not taken into account, even though it would make the calculation more accurate.

Change of material properties in a dependence on temperature, such as thermal conductivity and capacity, were taken into account according to chapters 7.3, 7.4 and 7.5. The numerical 2D model was done using ADINA Thermal software, using rectangular mesh with four nodes for surfaces, and two-nodal line mesh for edges, having the same length as rectangular mesh on surfaces.

For the analytical model MS Excel spreadsheet was developed according to procedure described in this thesis. This was done using iterative calculations for the heat transfer analysis, with time step equal to one minute.

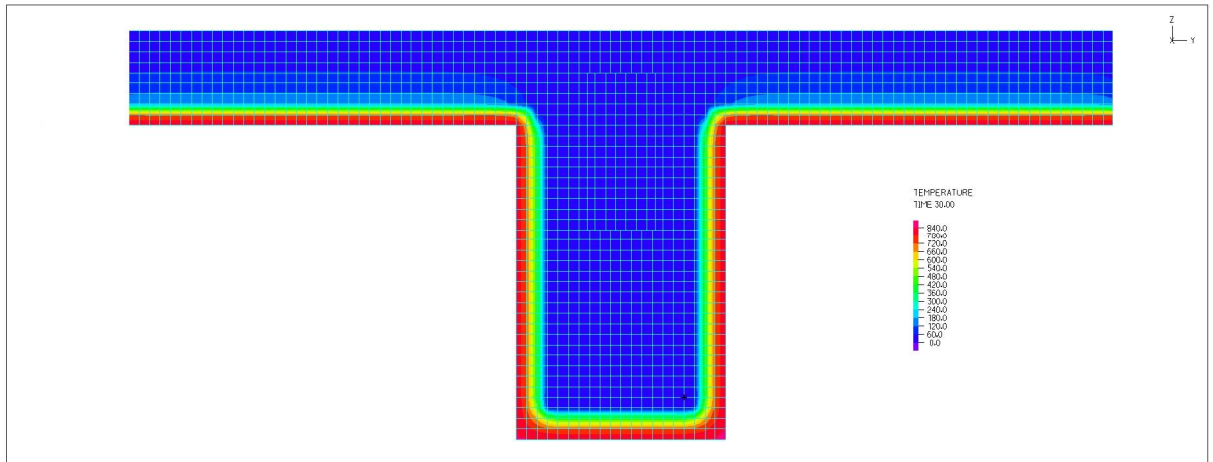


Figure 7.8: Temperature within the cross-section after 30 minutes of fire

The concrete layer is after 30 minutes of fire relatively cool due to good insulation of timber boards creating the interlayer. The burning of timber already takes place and therefore the timber cross-section as well as timber decking is reduced. The rounding of corners in the beam also takes place.

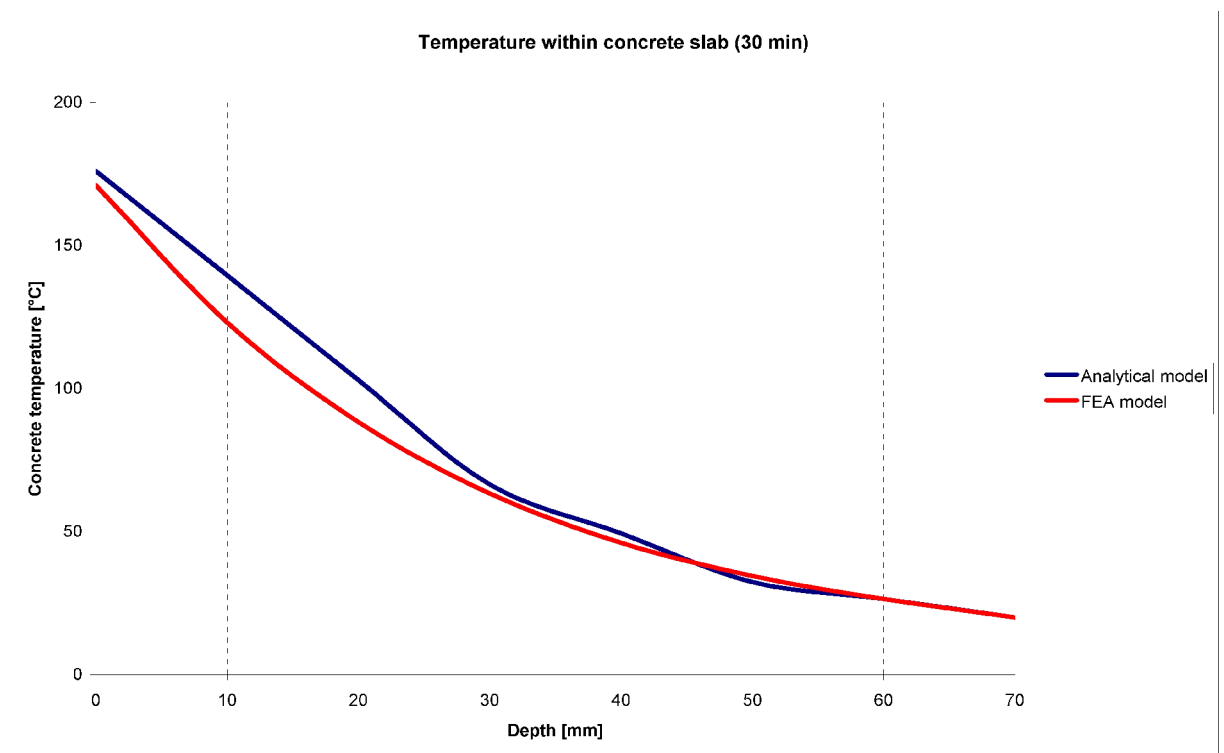


Figure 7.9: Comparison of numerical and analytical model results after 30 minutes of fire

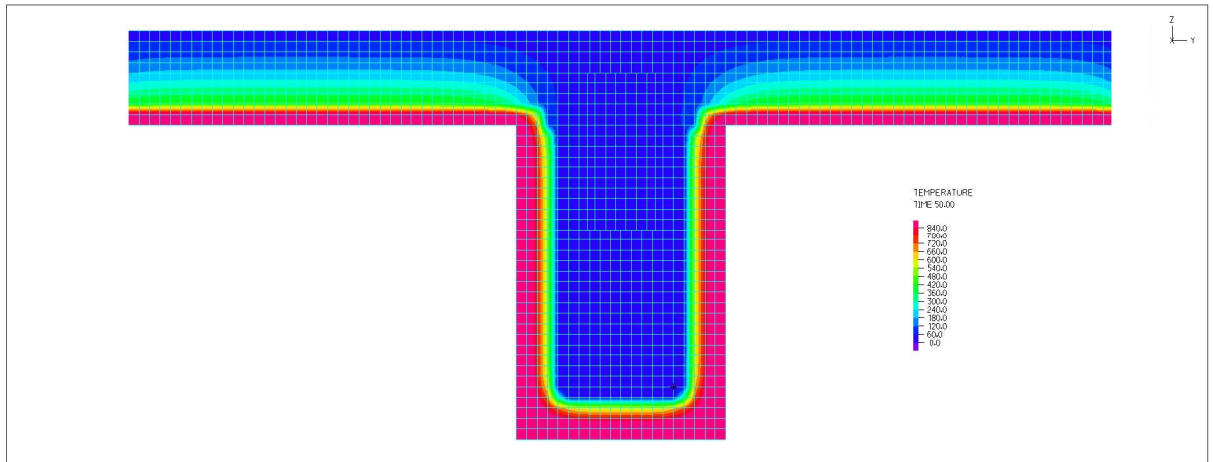


Figure 7.10: Temperature within the cross-section after 50 minutes of fire

After 50 minutes of fire the interlayer decking is almost burnt out, the cross-section of timber beam is reduced. Thermal gradient is much bigger in timber beam proving a good, and often underestimated, behaviour in fire. The strength and stiffness of concrete layer is reduced due to elevated temperature. In reality, spalling of concrete would probably take place.

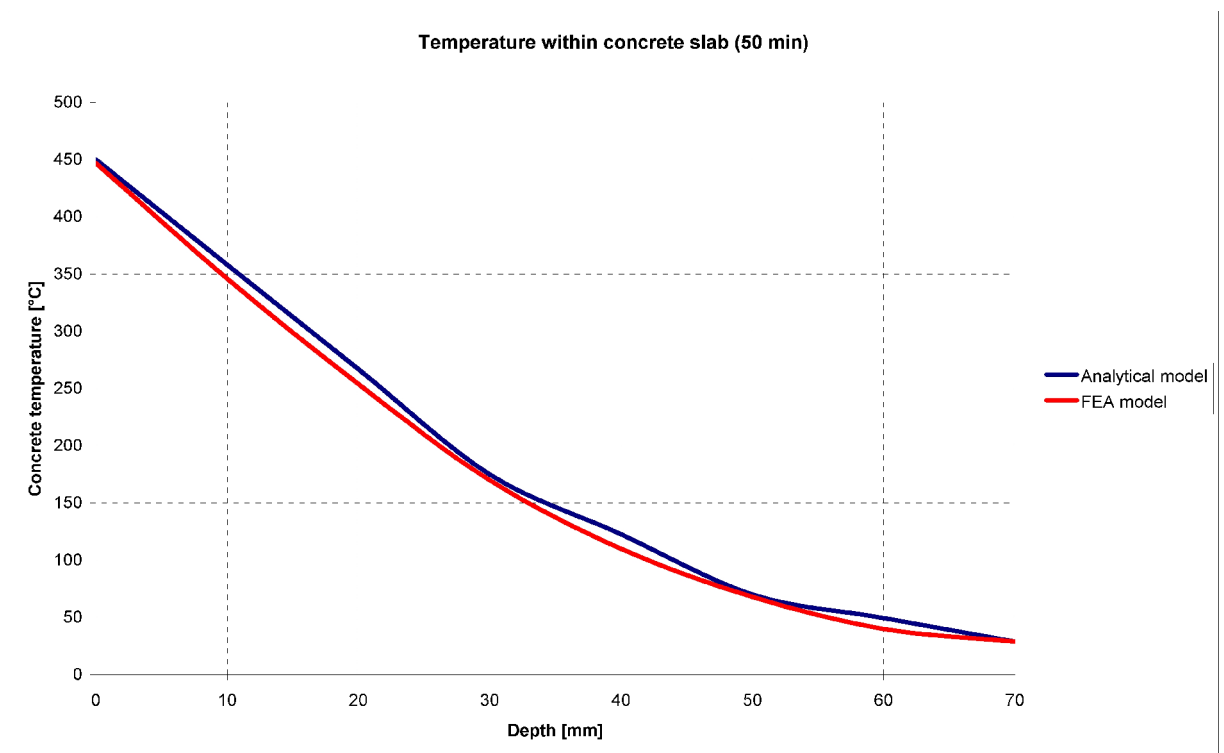


Figure 7.11: Comparison of numerical and analytical model results after 50 minutes of fire

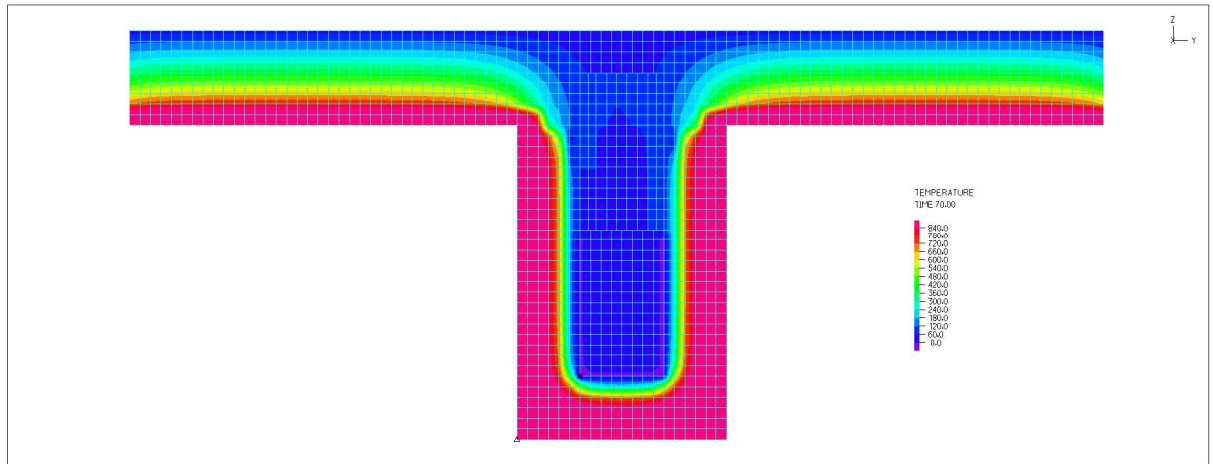


Figure 7.12: Temperature within the cross-section after 70 minutes of fire

After 70 minutes of fire the interlayer timber decking is completely burnt out, the timber beam is significantly reduced, concrete strength and stiffness is zero at the lower surface and significantly reduced in a big part of the cross-sectional area. Even the steel connectors are slightly heated up.

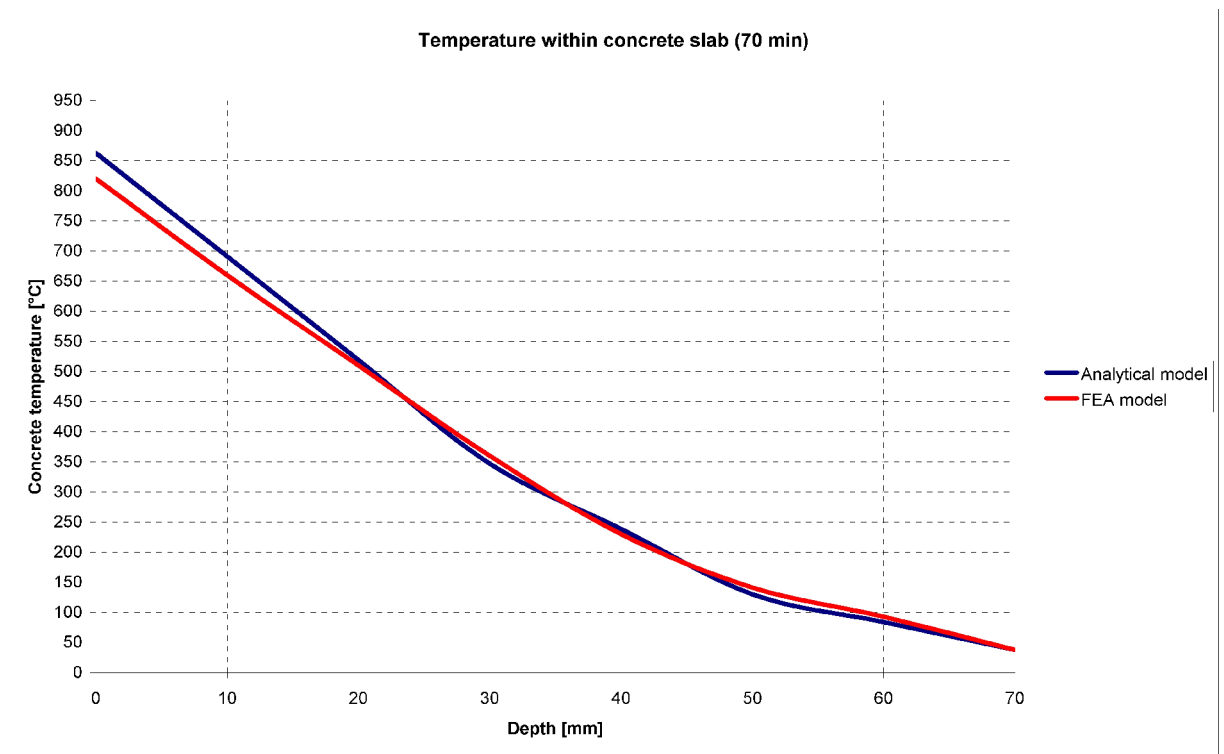


Figure 7.13: Comparison of numerical and analytical model results after 70 minutes of fire

The results of finite element analysis give similar results as indicated by analytical model. However, analytical model slightly differs with increasing time, giving rather conservative results though. Moreover, the influence of timber beam as insulation of the concrete slab is not considered in the proposed analytical model, providing the engineer a portion of safety to his design.

7.5.3 Load-Bearing Capacity of Concrete Component at Elevated Temperature

Strength and stiffness of concrete is significantly reduced with increasing temperature. The reduction factors used in proposed analytical calculation are based upon Eurocode 2, where the ratio $f_{c,\theta} / f_{ck}$ and elastic strain $\varepsilon_{cl,\theta}$ (see Table 1) are provided for several values of temperature θ_c . The behaviour can be than approximated by curves.

Table 7.1: Values for the main parameters of stress-strain relationships of normal-weight concrete with siliceous aggregates at elevated temperatures

Concrete temperature [°C]	$f_{c,\theta} / f_{ck}$	$\varepsilon_{cl,1}$
20	1,00	0,0028
100	1,00	0,0037
200	0,95	0,0052
300	0,85	0,0074
400	0,75	0,0105
500	0,6	0,0150
600	0,45	0,0250
700	0,3	0,0250
800	0,15	0,0250
900	0,08	0,0250
1000	0,04	0,0250
1100	0,01	0,0250
1200	0	0,0250

Data in Table 7.1 can be approximated by curves (modulus of elasticity is derived from elastic strain $\varepsilon_{cl,\theta}$). For the reduction of concrete strength following functions may be used¹:

$$\begin{aligned}
 k_{c,\theta} &= -1,7 \cdot 10^{-6} \theta^2 + 6 \cdot 10^{-5} \theta + 1,0047 & \text{for } 20^\circ\text{C} \leq \theta < 400^\circ\text{C} \\
 k_{c,\theta} &= -0,0015\theta + 1,35 & \text{for } 400^\circ\text{C} \leq \theta < 800^\circ\text{C} \\
 k_{c,\theta} &= 9,06 \cdot 10^{-7} \theta^2 - 0,0022\theta + 1,336 & \text{for } 800^\circ\text{C} \leq \theta < 1200^\circ\text{C}
 \end{aligned} \tag{7.24}$$

For the reduction of Young's modulus the following functions were derived:

$$\begin{aligned}
 k_{c,\theta} &= 2,7 \cdot 10^{-6} \theta^2 - 0,0032\theta + 1,0545 & \text{for } 20^\circ\text{C} \leq \theta < 600^\circ\text{C} \\
 k_{c,\theta} &= 1,75 \cdot 10^{-7} \theta^2 - 0,0004\theta + 0,2286 & \text{for } 600^\circ\text{C} \leq \theta < 1200^\circ\text{C}
 \end{aligned} \tag{7.25}$$

where $k_{c,\theta} = f_{c,\theta} / f_{ck}$ in case of the strength reduction and $E_{c,\theta} / E_{cm}$ in case of the reduction of Young's modulus.

Using the heat conduction analysis and functions for the strength and stiffness reduction we can get new properties of each layer, based on the temperature in the middle of this layer. However, it is much more convenient for the calculation to reduce the effective width of this layer (and thus the area of the layer). The new effective width of i^{th} layer is calculated as follows:

¹ These functions were obtained by approximation of curves. The accuracy is not perfect, but satisfactory. For engineering purposes it is also possible to make linear interpolation between values in Table 1.

$$b_{eff,\theta,i} = k_{c,\theta,i} \cdot b_c \tag{7.26}$$

where $k_{c,\theta,i}$ is the stiffness reduction factor from the equations (7.25). Where $b_{eff,\theta,i}$ is the effective width of each layer reduced by stiffness reduction coefficient $k_{c,\theta}$.

By this procedure the new centre of gravity of concrete component is obtained as:

$$\bar{z}_{c,eff,\theta} = \frac{S_{c,eff,\theta}}{A_{c,eff,\theta}} \tag{7.27}$$

where $S_{c,eff,\theta}$ is the first moment of area with respect to the lower surface of the concrete component and $A_{c,eff,\theta}$ is the effective area of the reduced cross-section of the concrete component.

The stiffness of concrete is considered to be constant through the reduced cross-section.

$$E_{cd,\theta} = \frac{E_{cm}}{\gamma_{c,fi}} \tag{7.28}$$

where E_{cm} is a mean value of initial tangent modulus of elasticity of concrete and $\gamma_{c,fi} = 1,0$.

The compressive strength varies through the concrete slab:

$$f_{cd,fi,i} = k_{c,\theta,i} \frac{f_{ck}}{\gamma_{c,fi}} \tag{7.29}$$

where $\gamma_{c,fi}$ is the partial safety factor for the relevant material property, $\gamma_{c,fi} = 1,0$; f_{ck} is the characteristic strength of concrete and $f_{cd,fi,i}$ is the strength of the i^{th} layer. However, in the proposed calculation the compressive strength only in the uppermost layer is compared with stress from the applied load. The tensile strength of concrete is neglected.

7.6 Strength and Stiffness of the Composite Cross-Section

After calculation of the effective cross-sectional dimensions (see figure 7.14), strength and stiffness at fire of timber beam and concrete slab, and reduction of strength and stiffness of connectors, the equations of the γ -method may be employed.

Using these equations we get new position of the neutral axis in the composite cross-section, new γ_{ct} stiffness coefficient, reduced bending stiffness of the cross-section $(EI_y)_{eff,\theta}$ and finally moment and shear resistance of the composite beam at elevated temperature.

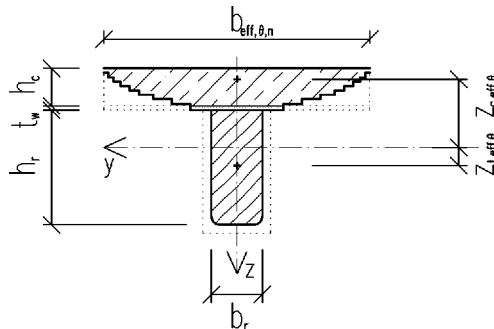


Figure 7.14: Effective cross-section in fire

The output of the calculation for the ultimate limit state is the critical stress in the cross-section. This critical stress is either compression of the concrete at the top fibres or tension in the timber beam or possibly shear stress in the timber beam. It is very unlikely to occur, but failure of concrete due to high shear force should be considered.

The critical failure mode gives us the smallest value of the moment and shear resistance which should be higher than applied load at fire:

$$\min \left\{ \begin{array}{l} M_{y,Rd,c,\theta} \\ M_{y,Rd,t,\theta} \end{array} \right\} \leq M_{Ed,fi} \quad \text{for the moment resistance}$$

$$\min \left\{ \begin{array}{l} V_{z,Rd,c,\theta} \\ V_{z,Rd,t,\theta} \\ V_{z,Rd,f,\theta} \end{array} \right\} \leq V_{Ed,fi} \quad \text{for the shear resistance} \quad (7.30)$$

If the connection fails, it does not mean that the entire structure loses its load-bearing function. In that case the components of a cross-section begin to act independently with zero composite action and the load-bearing resistance is reduced. However, since the loading at fire is reduced, it can still carry the load, only the deflection will instantly increase. The values of moment and shear resistance can be obtained analogically to ones mentioned in chapter 6, using the modified geometry, stiffness, strength and stiffness coefficient according to procedure mentioned therein before.

This should be done using iterative approach, when all the procedure is repeated for each minute of fire development. It is almost impossible to perform such calculation in hand-calculation; therefore it is convenient to make a spreadsheet application.

7.7 Comparison of Results with Full-Scale Laboratory Tests

In order to study the global behaviour of timber-concrete composite slabs with interlayer slip, a full-scale fire test at ETH in Zurich was performed with the slab shown in figure 7.15.

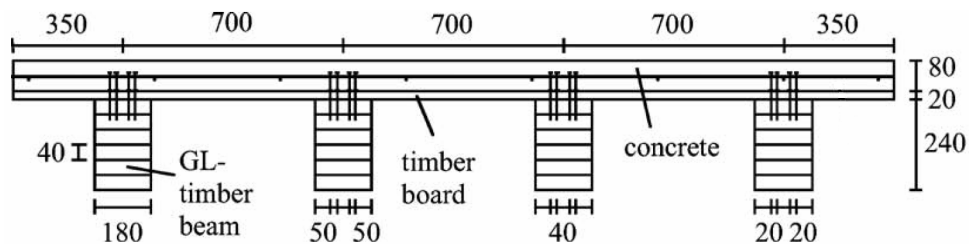


Figure 7.15: Cross-section of the timber-concrete composite slab tested under ISO fire exposure

The 180 mm wide and 240 mm high timber beams consisted of glulam GL24h according to EN 1194. The density of the timber beams varied between 431 and 445 kg/m³ and the mean value of moisture content was about 13%. The modulus of elasticity of each timber beam was measured before the composite slab was prepared. The mean value of the modulus of elasticity of the timber beams was 10 620 MPa. The measured modulus of elasticity of the concrete slab was 37 000 MPa and the cylindrical compressive concrete strength was 47 MPa. The spacing of the screws was 120 mm and the timber side cover 50 mm.

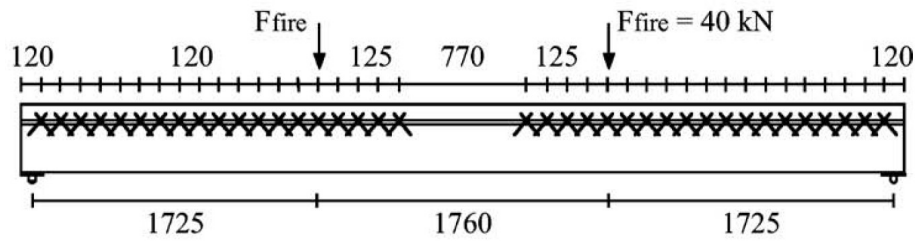


Figure 7.16: Longitudinal section of the timber-concrete composite slab tested under ISO fire exposure

The slab was designed for a fire resistance of 60 min. The slab was loaded with hydraulic jacks at about a third of the span (see figure 7.16). During the fire test the vertical deflection as well as the slip between concrete slab and timber beams increased as the fire progressed due to loss of cross-section as well as the influence of temperature on the stiffness of timber and connection.

The slab finally failed after 67 min of ISO fire exposure due to failure of the screwed connection and successively failure of the glulam beams. The fire behaviour of the composite slab was calculated according to the model explained in the previous paragraphs. For the calculation, mean values of strength and stiffness properties of timber, concrete, and connection were used. The calculation model predicted a fire resistance of 63 min, which agreed very well with the fire resistance measured. The calculation model also correctly predicted the failure mode of the composite slab. The calculated vertical deflection (see figure 7.17) was slightly smaller in the beginning, but higher from 45th min.

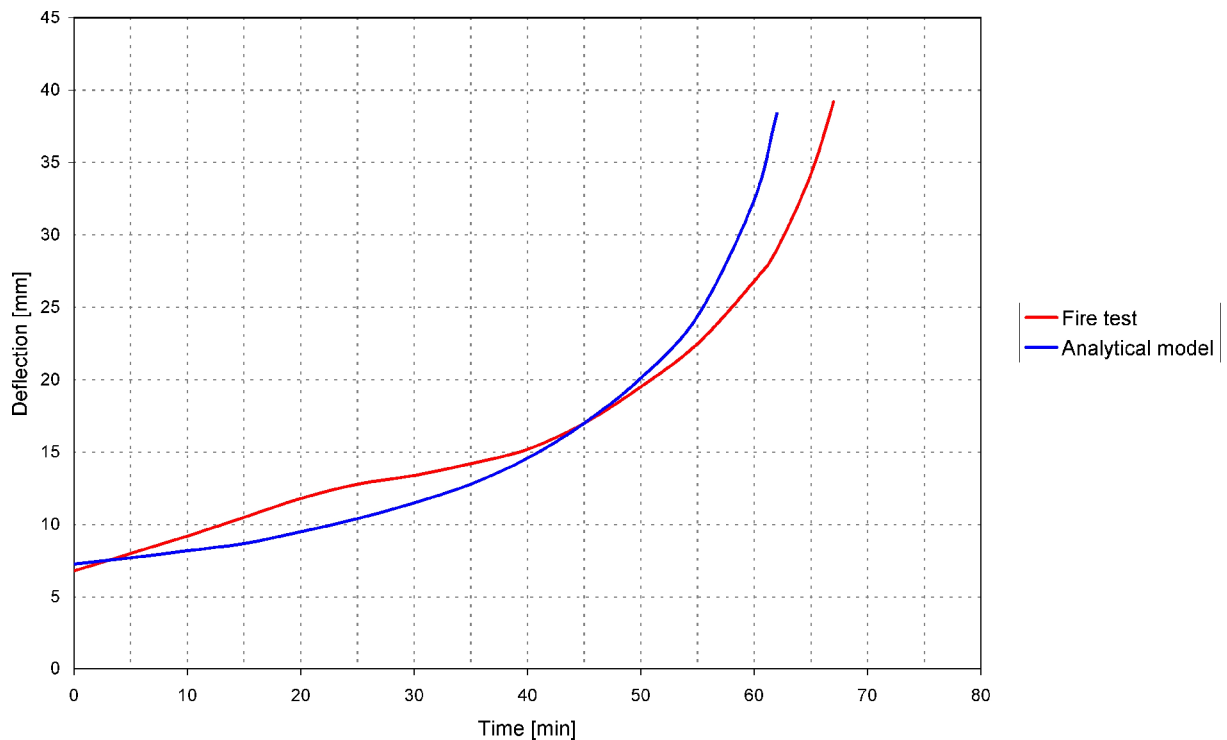


Figure 7.17: Comparison of calculated and measured deflection

8 Comparison of Timber-Concrete Composite and RC Floor

The comparative study is based on realistic boundary conditions, which are same for both systems, including loading and supporting. The span for both systems is 7 500 mm in one direction, the second direction is not important since both are one-way systems. Concrete class is also the same, C30/37. Both floors are loaded by live load $q_k = 5 \text{ kNm}^{-2}$ and imposed dead load $g_k = 2 \text{ kNm}^{-2}$ plus self-weight of the floor structure itself. Serviceability limit state including deflection, vibrations and cracking is not investigated.

The design of timber-concrete composite floor is done according to procedure described in this thesis, chapter 6. Reinforced concrete floor is designed according to EN 1992-1-1. The design of both systems is done in such a way to be economic and realistic.

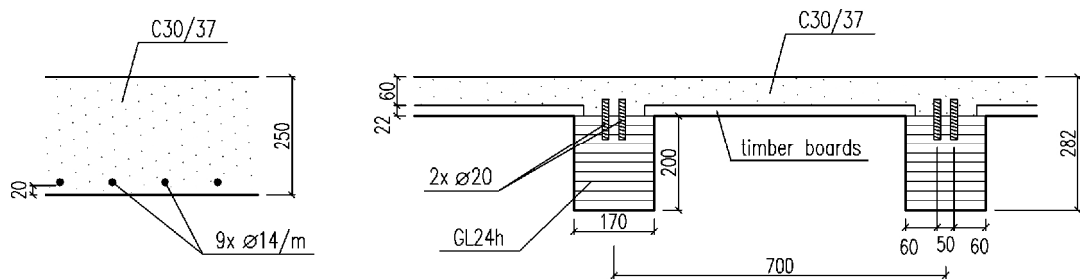


Figure 8.1: Cross-section of RC floor (left) and timber-concrete composite floor (right)

8.1 RC Floor Design and Performance

From the empirical formulas, thickness of the concrete slab was designed as 250 mm thick, adding a great portion of dead-load in form of self-weight. The maximum design moment is then $M_{Ed} = 128,7 \text{ kNm}$ per meter of width. With the given slab thickness and concrete class C 30/37, the resulting force in reinforcement is $F_s = 602 \text{ kN}$ per meter of width. For such tensile force 9 rebars per meter with diameter of 14 mm is a reasonable choice, resulting in 2,9 % of reserve and satisfactory geometric reinforcement ratio. Secondary reinforcement is designed as 7 rebars per meter with diameter 7 mm.

Relatively high self-weight of the floor results in big requirements on the supporting vertical structure and foundations. The advantage of such floor is quite good behaviour in fire. Fire resistance of the RC slab is assed according to the zone method from EN 1992-1-2.

The bending moment in fire situation is reduced to $M_{Ed,fi} = 73,8 \text{ kNm}$ per meter of width, reduction factor for live load is taken as $\psi_{2,1} = 0,5$. The reduction of stress carried by reinforcing steel begins to decrease at 40th minute of fire, when temperature in steel reaches 313°C. At the time of predicted collapse of the concrete slab, the temperature in steel reaches 608°C and reduction coefficient $k_{s,\theta} = 0,45$. At this time the effects of elevated temperature in concrete do not have to be considered, because the upper surface of the concrete slab does not reach 100°C. Therefore the requirement on insulation is automatically fulfilled. Shear resistance is checked by means of minimal allowable thickness from tables. Spalling of concrete should not have any significant effect, since the slab is situated in a dry environment.

According to calculation, the fire resistance of RC floor is 123 min and therefore fulfils the requirement REI 120.

8.2 Design and Performance of Timber-Concrete Composite Floor

Beams in composite floor are designed as glulam GL24h with height 200 mm and width 170 mm and the distance between timber beams is 700 mm. Timber decking, providing a formwork for concrete slab, is made of timber boards with a thickness of 22 mm. The thickness of slab is designed as 60 mm, concrete class is the same as in the previous case, C 30/37. To avoid cracking, a steel mesh should be placed at the lower surface of the concrete slab. However, this is not taken into account in the calculation. Shear connection is provided by means of dowel-type fasteners with an ultimate strength $f_u = 900$ MPa and the diameter 20 mm. Spacing of fasteners is $s_{min} = 50$ mm near supports and $s_{max} = 100$ mm at midspan. It provides the connection with a slip modulus $K_u = 10\,592$ Nmm⁻¹. The connection efficiency factor $\gamma_{ct} = 0,61$.

The maximum design shear force near supports reaches $V_{Ed} = 31,7$ kN, resulting in maximum shear stress in the timber beam $\tau_{t,max} = 1,3$ MPa. Reserve for the shear force is therefore 38,2 %. The maximum design bending moment is $M_{Ed} = 59,5$ kNm per T-section width, resulting in reserve 8,5 %.

Compression in concrete is a decisive factor, followed by tension in the lower fibres of timber beams, where the reserve is 12,3 %. The distribution of normal stress within the composite cross-section is illustrated in the figure 8.2:

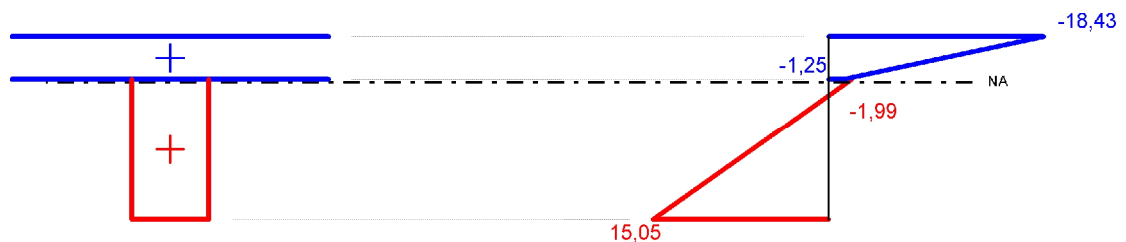


Figure 8.2: Distribution of normal stress within the composite cross-section at room temperature

The small thickness of the concrete slab and combustibility of timber beams results in lower fire resistance in comparison with RC floor. However, since the dead load on such structure is also lower. The fire reduction coefficient $\eta_{fi} = 0,49$ gives a bigger reduction of internal forces than in the case of RC floor, where the fire reduction coefficient reached only the value of $\eta_{fi} = 0,58$. Taking into account the same live load reduction factor $\psi_{2,1} = 0,5$ as for the RC floor, the bending moment in fire situation is reduced to $M_{Ed,fi} = 29,0$ kNm per width of T-section.

Fire resistance of the composite floor, assessed according to the method described in this thesis, is 62 min and therefore fulfils the requirement REI 60. The structure is expected to fail because of the loss of the bending moment resistance.

Assessment of the shear force resistance is rather conservative, considering only the timber beams to be effective. However, even with such assumption the shear stress is not decisive factor for evaluation of the fire resistance. The shear failure of the timber beam would, according to the calculation, occur in 79th minute. The maximal deflection at the time of failure at 62nd minute is calculated to be 89,1 mm.

The following graphs describe behaviour of timber-concrete composite floor in fire and comparison with RC floor.

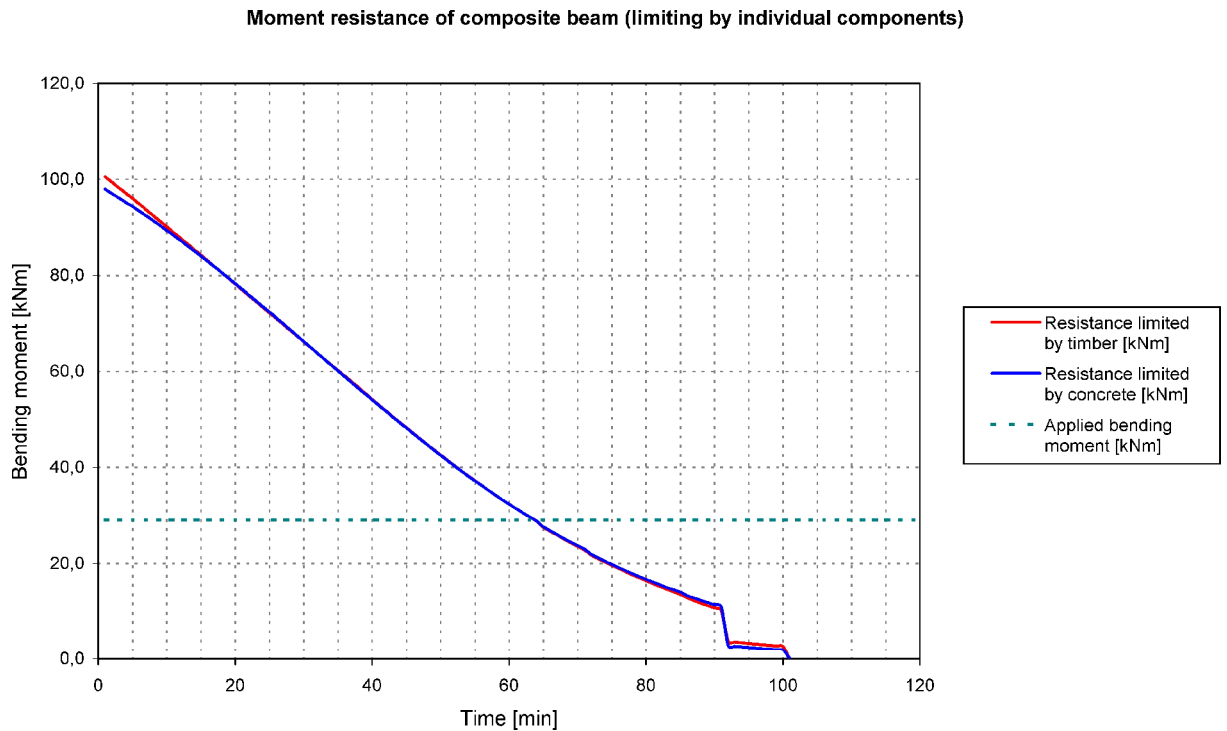


Figure 8.3: Limitation of moment resistance by individual components

The loss of load-bearing capacity for both components has almost the same course. It means that the cross-section is perfectly balanced and the best possible performance is reached. The reduction of strength and stiffness of shear connectors may be observed from 90th minute. From that time on, the section is not composite and the components, i.e. concrete slab and timber beam, are independent.

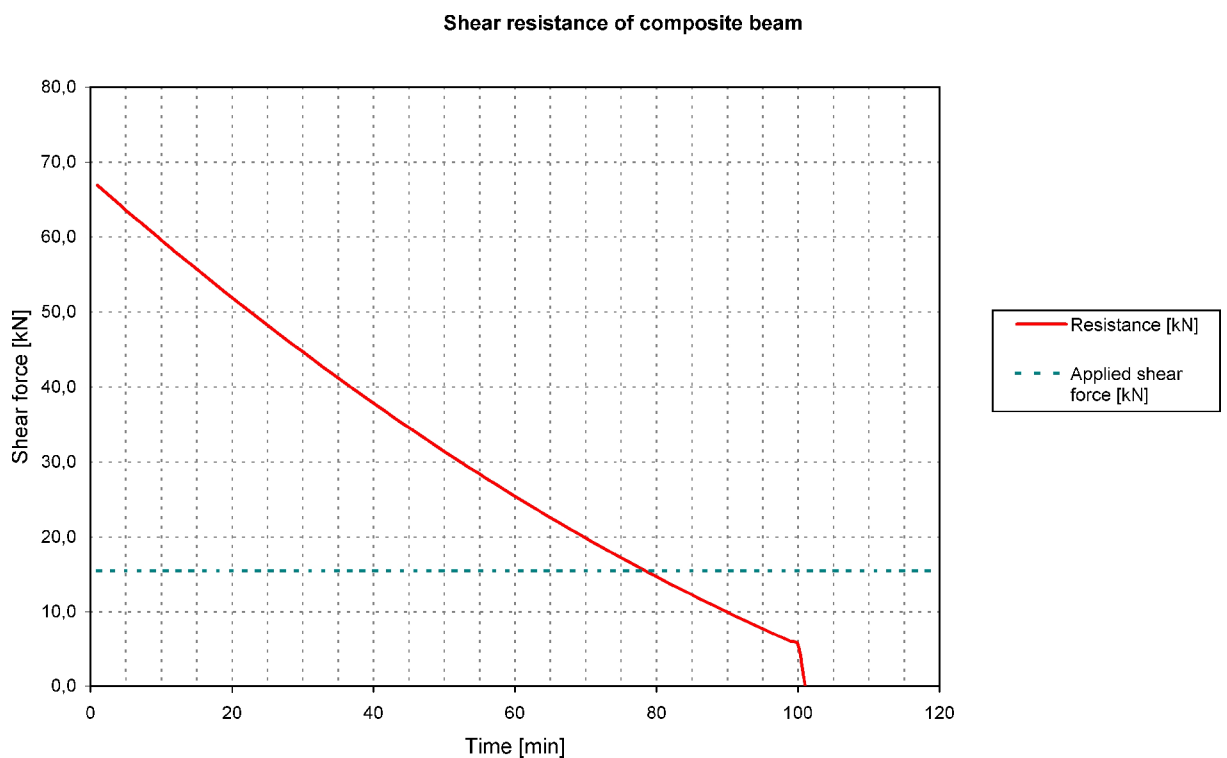


Figure 8.4: Shear resistance of the composite beam

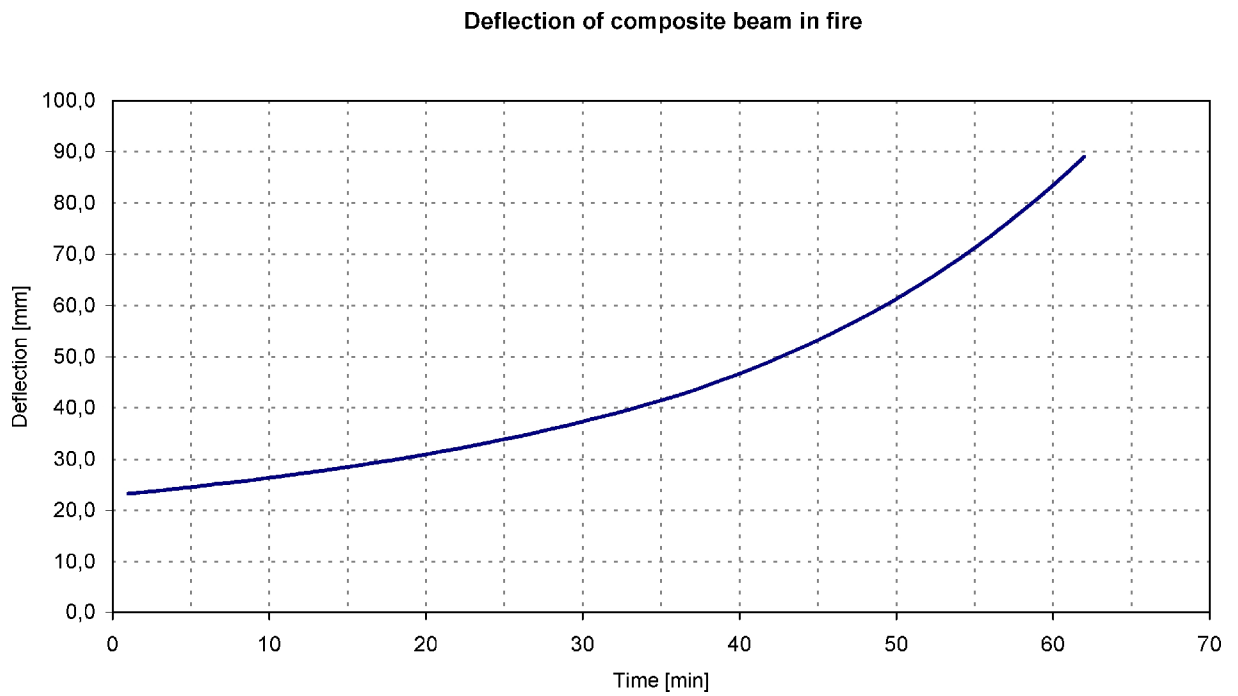


Figure 8.4: Course of deflection during fire

The deflection is influenced by the loss of stiffness of concrete and decreasing moment of inertia due to charring of timber beam. Therefore rather high values are reached before the collapse of the structure. If the loss of strength of connectors occurred before failure, the deflection would instantly increase at that moment.

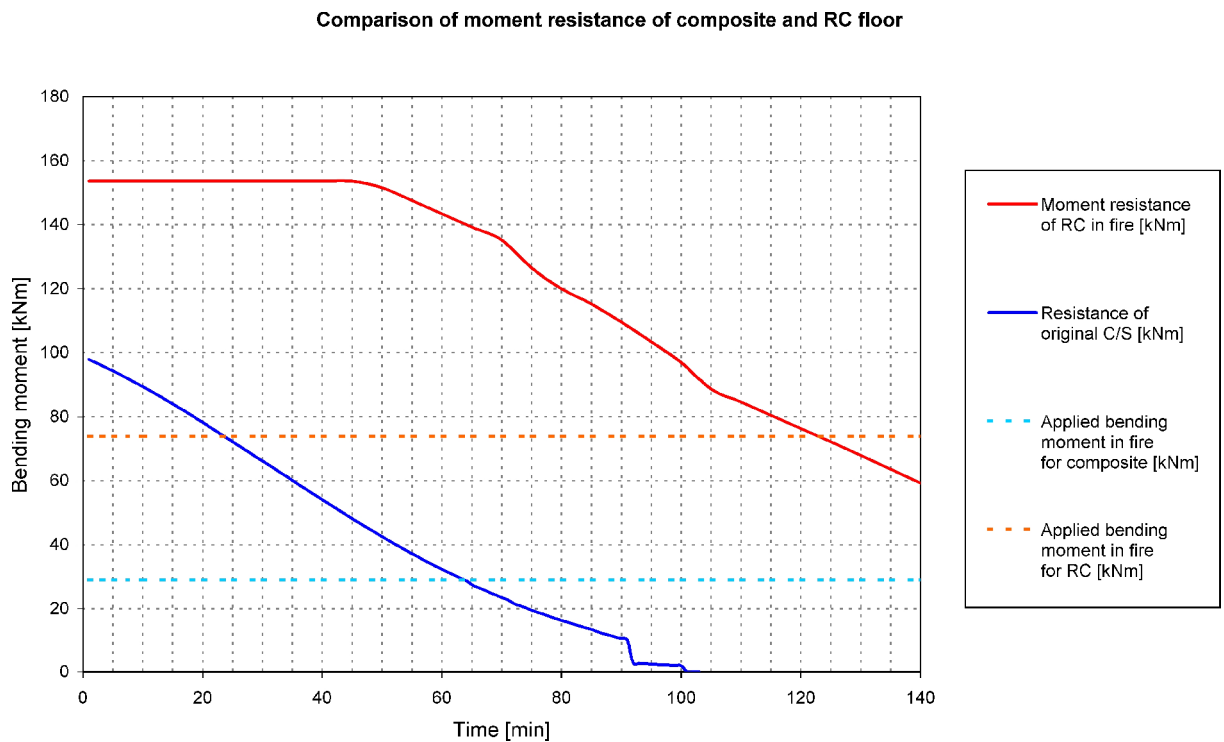


Figure 8.5: Comparison of the fire resistance of timber concrete composite and RC floor

The better fire resistance of the RC floor is depicted in figure 8.5. The timber-concrete composite has significantly lower load-bearing capacity at any time, but it is also less loaded due to reduced self-weight. The load-bearing capacity of composite floor is decreasing from the very first minute of fire, because of charring of timber beams. On the other hand, the moment resistance of RC floor is decreasing from the moment, when the temperature in steel causes reduction of stress carried by reinforcement.

8.2.1 Cross-Section Optimization for Better Performance in Fire

To reach a significantly better performance, small changes in geometry of composite cross-section can be made.

Design of timber beam with a higher cross-section increases the moment of inertia of the beam at any time of fire. A bigger width contributes to the extended life-time of the timber beam, since it takes longer time to burn it away. Increased thickness of the interlayer decking has better insulation properties and therefore the concrete slab is protected from fire. It also increases the lever arm between tensile force in timber beam and compressive force carried by concrete. Finally, designed bigger thickness of concrete slab contributes to bigger stiffness of the whole structure and it is also necessary to balance the modification of timber part.

To exploit all positive effects from the above mentioned modification, shear connectors have to be placed in a sufficient distance from the beam edge to avoid loss of their stiffness and therefore separation of both components, before the floor reaches its failure as a partially composite structure.

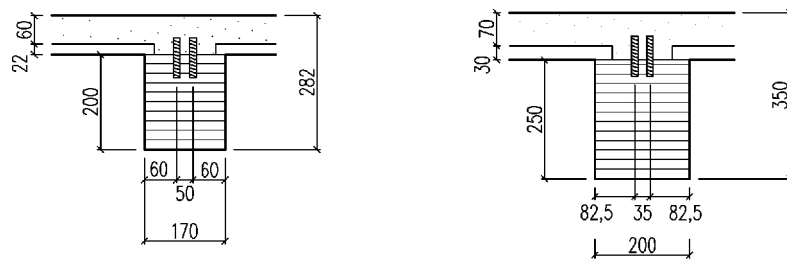


Figure 8.6: Original and modified cross-sections

To give an example, the geometry of cross-section investigated in the previous chapter is modified according to figure 8.6. The span, imposed loading and the distance between timber beams is unchanged. Width of timber beams is increased by 30 mm and height by 50 mm. Thickness of the interlayer was increased by 8 mm and thickness of the concrete slab by 10 mm. It results in slightly higher self-weight and therefore increased loading. The load at fire situation is then $M_{Ed,fi} = 31,0$ kNm and $V_{Ed,fi} = 16,5$ kN per width of T-section. This change is really small in comparison with the positive effect on load-bearing capacity of the composite cross-section.

To fully exploit the modifications in geometry, shear connectors should be moved towards the vertical axis of timber beams. Materials of the cross-section are the same for both cases

At a room temperature, compression in concrete is a decisive factor for a moment resistance. Reserve of the modified cross-section is 70,7 % and even higher reserve is in shear resistance. For the design at room temperature, the cross-section is not fully exploited and therefore such design would be considered as uneconomical. However, the performance in fire is significantly improved.

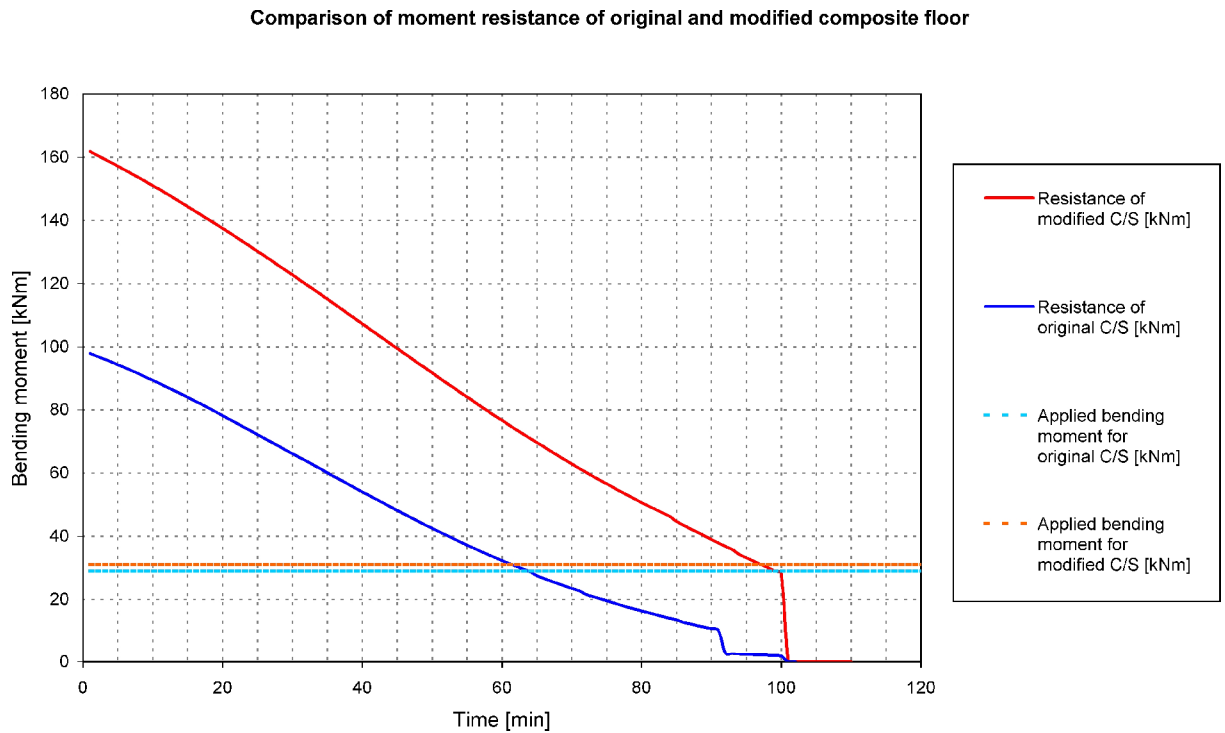


Figure 8.7: Comparison of the floor fire resistance with original and modified cross-sections

After modifications in geometry the increase in imposed load due to higher self-weight is negligible (see figure 8.7). However, the performance of modified floor is much better. The new structure would, according to calculations, fail at 96th minute due to loss of moment resistance and the maximal deflection would be 76,5 mm. The loss of stiffness in shear connection may be observed after the expected failure of the structure and therefore the distance of connectors from the edge of timber beams is sufficient.

The modified structure would easily fulfil the requirement of REI 90.

9 Conclusion

Timber-concrete composite floors have many advantages over traditional timber floors and even over reinforced concrete systems. They are economic to build, easy to construct and very effective as stiff systems. Moreover, timber-concrete composites provide a nice architectural appearance and have great possibilities in today's construction market for new and renovated buildings, and bridges.

For design purposes a simplified linear-elastic calculation model (γ -method) is widely used. The results of bending tests showed that the γ -method gives a satisfactory prediction of the behaviour until the plastic range is reached. To make the design of a timber-concrete composite floor reasonable and economic, the structural behaviour of composite section must be well understood. The use of an application, programmed for example in MS Excel, can significantly speed up the design and verification process. Such application also enables to fully optimize the design for a given boundary conditions.

The behaviour of timber-concrete composite structures is governed by the shear connection between timber and concrete. Therefore effective systems that are relatively cheap should be developed to replace rather ineffective and unpredictable traditional dowel-type fasteners. The newest methods of connection by adhesives are being developed, promising a rise in popularity of timber-concrete composites.

Big obstacle for structures consisting of timber members is that they are generally considered to be very bad in fire. However, a low self-weight of such structures provides quite good performance.

The performance of timber-concrete floors in fire is particularly good, because the upper concrete slab is an efficient barrier against fire propagation that increases fire resistance compared to all-timber systems. In addition, timber ribs are more fire-resistant than those of steel or pre-fabricated pre-stressed concrete. Moreover, performance of timber-concrete composite floor in fire can be significantly improved by only a small, but balanced change in cross-sectional dimensions.

For the calculation of the fire resistance of timber-concrete composite slabs a simplified design method was developed on the basis of γ -method for mechanically jointed beams with flexible elastic connections. The fire design can be performed using the effective cross-section and modifications taking into account the effects of temperature on mechanical properties of timber, concrete, and connection.

For the strength and stiffness properties of the screwed connections simplified formulae for the calculation of the modification factors $k_{mod,fi}$ were developed, based on the results of the fire tests at ETH in Zurich. The modification factors were expressed as a function of the side cover of the connectors. Tests for other types of connectors should be also made to help the engineers with fire design of timber-concrete composites connected by other technology.

The fire resistance predicted by the simplified calculation model agreed very well with the resistance measured in the full-scale fire test.

Notation

$(EI_y)_{eff,\theta}$	effective bending stiffness of composite cross-section at temperature θ
A_c	effective area of concrete
$A_{c,eff,\theta}$	effective area of concrete at temperature θ
A_r	area of residual timber cross-section
A_t	area of timber
b_c	width of concrete flange
b_{eff}	effective width of concrete
$b_{eff,\theta,i}$	effective width of i^{th} layer of concrete at temperature θ
b_t	width of timber beam
c	specific heat capacity of material
d	diameter of dowel-type fastener
d_{char}	charring depth
E	modulus of elasticity (Young's modulus)
E_c	modulus of elasticity of concrete
$E_{c,\theta}$	modulus of elasticity of concrete at temperature θ
E_{cm}	mean modulus of elasticity of concrete
EI_{eff}	effective stiffness of composite cross-section
E_{mean}	mean value of modulus of elasticity of timber
E_t	modulus of elasticity of timber
$f_{c,\theta}$	compressive strength of concrete at temperature θ
$f_{i,d}$	design strength of i^{th} subcomponent
$f_{i,k}$	characteristic strength of i^{th} subcomponent
$F_{v,Ed}$	force on fastener
$F_{v,Ed,fi}$	design load on connector in fire
$F_{v,Rd}$	resistance of fastener
F_s	force in reinforcing steel
h_c	thickness of concrete slab
$h_{net,c}$	convective heat flux
$h_{net,r}$	heat flux from radiation
h_t	height of timber beam
I_c	moment of inertia of concrete component
I_t	moment of inertia of timber component
K	slip modulus
k	slip modulus per-unit-length (smeared modulus)
$k_{c,\theta}$	reduction coefficient at temperature θ
k_{def}	timber creep coefficient
k_{fi}	coefficient converting 5 th fractile value to 20 th fractile value
k_{mod}	modification factor reducing strength of material
$k_{mod,fi}$	modification factor of strength or stiffness in fire
K_{ser}	slip modulus for serviceability limit state
$K_{ser,fin}$	long-term final slip modulus
K_u	slip modulus for ultimate limit state
l_{eff}	effective span (length of timber beam)
M_c	moment carried by concrete layer
M_{Ed}	applied moment
$M_{Ed,fi}$	applied moment at fire
M_t	moment carried by timber beam
$M_{y,Rd}$	design moment resistance around y-axis

$M_{y,Rk}$	characteristic moment resistance around y-axis
N_c	normal force carried by concrete
n_c	ratio of moduli of elasticity (stiffness reduction factor)
N_t	normal force carried by timber
p	perimeter of residual timber cross-section
Q	heat energy
$R_{fi,d,t}$	loading of member in fire at time t
$R_{fi,d,t}$	resistance of member in fire at time t
s	spacing of connectors
$S_{c,eff,\theta}$	effective moment of area of concrete at temperature θ
s_{eff}	effective spacing
$S_{y,i}$	first moment of area of i^{th} subcomponent
T	shear force between components
t	time
t_w	thickness of interlayer
u	displacement in direction of x-axis
V_{Ed}	applied shear force
$V_{Ed,fi}$	applied shear force at fire
V_z	shear force in direction of z-axis
$V_{z,Rd,i}$	design shear force resistance around z-axis for i^{th} subcomponent
$V_{z,Rk,i}$	characteristic shear force resistance around z-axis for i^{th} subcomponent
w	displacement in direction of z axis
x	timber side cover of connectors
z_c	distance from overall neutral axis to centre of gravity of concrete slab
z_t	distance from overall neutral axis to centre of gravity of timber beam
α	coefficient of long-term effects on concrete
α_c	convective heat transfer coefficient
β_n	charring rate of timber
γ_C	partial safety factor for concrete
γ_{ct}	connection stiffness coefficient
γ_M	partial safety factor for timber and connectors
ε_m	emissivity coefficient
η_{fi}	reduction factor for design load level at fire situation
θ	temperature
θ_g	gas temperature in fire compartment
θ_m	temperature of radiation receiving body
θ_r	temperature of emitting body
λ	thermal conductivity coefficient
$v_{R,k,l}$	characteristic shear strength of concrete
ρ_m	mean density of timber
σ	Stefan-Boltzmann constant
σ_i	stress in i^{th} subcomponent
τ_i	shear stress in i^{th} subcomponent
Φ	situation factor of surface in fire
ψ_2	live load reduction factor

References

- ADINA, *User Interface Command Reference Manual, Volume II: ADINA Heat Transfer Model Definition*, Report ARD 09-3, 2009
- ADINA: *User Interface Command Reference Manual Volume I: ADINA Solids & Structures Model Definition*, Report ARD 09-2, 2009
- BATHE K.J.: *Finite Element Procedures in Engineering Analysis*, Prentice-Hal Inc., 1982
- BUCHANAN A.: *Fire performance of timber construction*, Prog.Struct.Eng.Mater, 2000
- ČAS B., SAJE M., PLANINC I.: *Nonlinear finite element analysis of composite planar frames with inter-layer slip*, Computers and Structures, 2004
- CECCOTTI A.: *Timber-concrete composite structures*, Timber engineering STEP2, Centrum Hout (NL), 1995
- CHUAN D., FRAGIACOMO M., ALDI P., MAZZILLI M., KUHLMANN U.: *Performance of Notched Coach Screw Connection for Timber-Concrete Composite Floor System*, NZ Timber Design Journal, Vol.17, No.1
- CLOUSTON P., CIVJAN S., BATHON L.: *Experimental behavior of a continuous metal connector for a wood-concrete composite system*, Forest Products Journal, Vol.54, No.69, 1999
- EN 1991-1-2 (Eurocode 1): *Actions on structures, Part 1-2: Actions on structures exposed to fire*, Commission of the European Communities, Brussels, 2002
- EN 1992-1-1 (Eurocode 2): *Design of timber structures, Part 1-1: General rules - Common rules and rules for buildings*, Commission of the European Communities, Brussels, 2004
- EN 1992-1-2 (Eurocode 2): *Design of concrete structures, Part 1-2: General rules – Structural fire design*, Commission of the European Communities, Brussels, 2004
- EN 1995-1-1 (Eurocode 5): *Design of timber structures, Part 1-1: General rules - Common rules and rules for buildings*, Commission of the European Communities, Brussels, 2004
- EN 1995-1-2 (Eurocode 5): *Design of timber structures, Part 1-2: General rules - Structural fire design*, Commission of the European Communities, Brussels, 2004
- FAGGIANO B., MARZO A., MAZZOLANI F.M., CALADO L.M.: *Analysis of rectangular-shaped collar connectors for composite timber-steel-concrete floors: Push-out tests*, Journal of Civil Engineering and Management, 2009
- FRANGI A., FONTANA M.: *A design model for the fire resistance of timber-concrete composite slabs*, Proceedings of the IABSE Conference on Innovative Wooden Structure and Bridges, Lahti, Finland, 2001
- FRANGI A., FONTANA M.: *Elasto-Plastic Model for Timber-Concrete Composite Beams with Ductile Connection*, Structural Engineering International, Vol.13, No.1, 2003.
- FRANGI A., KNOBLOCH M., FONTANA M.: *Fire Design of Timber-Concrete Composite Slabs with Screwed Connections*, Journal of Structural Engineering, Vol.136, No.2, 2010.
- GUTKOWSKI R.M., BROWN K., SHIGIDI A., NATTERER J.: *Investigation of notched composite wood-concrete connections*, Journal of Structural Engineering, 2002
- HEIDARPOUR A., BRADFORD M.A.: *Generic non-linear modelling of a bi-material composite beam with partial shear interaction*, International Journal of Non-Linear Mechanics 44, 2009
- HUANG Z., BURGESS I.W., PLANK R.J.: *Behaviour of reinforced concrete structures in fire*, 2007
- KAVALIAUSKAS S., KVEDARAS A., GURKŠNYS K.: *Evaluation of Long-Term Behaviour of Composite Timber-Concrete Structures According to EC*, Ukio technologinis ir ekonominis vystymas, Vol. 9, No.4, 2005
- LE BORGNE M.R., GUTKOWSKI R.M.: *Effects of various admixtures and shear keys in wood-concrete composite beams*, Construction and Building Materials, 2010

- MIKE J.: *Analytical Methods to Evaluate Fire Resistance of Structural Members*, Journal of Structural Engineering, 1999
- PORTEOUS J., KERMANI A.: *Structural Timber Design to Eurocode 5*, Blackwell Publishing Ltd., 2007
- RACHER P., LAPLANCHE K., DHIMA D., BOUCHAÏR A.: *Thermo-mechanical analysis of the fire performance of dowelled timber connection*, Engineering Structures 32, 2010
- RONCA P., GELFI P., GIURIANI E.: *The behaviour of a wood-concrete composite beam under cyclic and long term loads*, Proceedings of the 2nd International Conference STREMA, Seville, May 1991
- SCHNABL S., PLANINC I., TURK G., SPRČIČ S.: *Fire analysis of timber composite beams with interlayer slip*, Fire Safety Journal 44, 2009
- TAJNIK M., DOBRILA P., PREMROV M.: *Analysis of Composite T-Beam Composed of Timber, Concrete and Carbon Strip*, University of Maribor, 2007
- VAN DER LINDEN M.: *Timber-Concrete Composite Beams*, Heron-English Edition, 1999